American Mineralogist, Volume 73, pages 1235–1254, 1988

Electrical conductivity of diopside: Evidence for oxygen vacancies

J. Stephen Huebner, Donald E. Voigt*

U.S. Geological Survey, Reston, Virginia 22092, U.S.A.

Abstract

Impedance spectra for two natural single crystals of diopside were obtained at 800 to 1300 °C and 1-bar pressure over the frequency range 0.001 Hz to 100 kHz in a system closed to all components but oxygen. For the near–end-member composition, approximately $Na_3Ca_{96}Mg_{96}Fe_3Al_2Si_{200}O_{600}$, over the $\log f_{O_2}$ (f_{O_2} in bars) range -9 to -14 at 1000 °C and -8 to -12 at 1200 °C, a range exceeding that of most igneous and metamorphic processes, the conductivity (σ, in units of siemens per meter) for three crystallographic orientations at 1-bar pressure is given by

$$(100): \log \sigma = 1.43 - 10850/T - 0.18 \log f_{O_2},$$
$$(010): \log \sigma = 0.88 - 10170/T - 0.12 \log f_{O_2},$$
$$(001): \log \sigma = 1.58 - 11080/T - 0.15 \log f_{O_2},$$

where T is in kelvins. The activation energy is 2.1 eV. At both higher and lower f_{O_2} values, no f_{O_2} dependence of conductivity was observed, indicating the presence of different conduction mechanisms. At temperatures less than 1000 °C, the activation energy is 1.3 eV, also suggesting a different conduction mechanism. Thus, at least four regimes are necessary to describe the conductivity of this diopside in T-f_{O_2} space. The approximately $-1/(7 \pm 1)$ value of $\partial(\log \sigma)/\partial(\log f_{O_2})$ in the high-temperature geologic region suggests a reaction by which oxygen vacancies control the conductivity. This relatively pure diopside is much less conducting than olivine $(Mg,Fe)_2SiO_4$ or orthopyroxene $(Mg,Fe)_2Si_2O_6$.

A second diopside with greater Fe content ($Na_2Ca_{96}Mg_{85}Fe_{12}Al_3Si_{199}O_{600}$), but otherwise similar in composition to the near–end-member diopside, is more conducting, has a smaller activation energy (1.0 eV) over the range 1050 to 1225 °C, and shows only a weak negative f_{O_2} dependence:

$$(100): \log \sigma = -0.89 - 4640/T - 0.03 \log f_{O_2},$$
$$(010): \log \sigma = -0.25 - 5270/T - 0.02 \log f_{O_2},$$

where T is in kelvins, suggesting that oxygen vacancies are present but are not the dominant defect in controlling the conductivity.

It is probable that oxygen vacancies are also present in pyroxenes in nature, even though they may not be the dominant point defects in natural assemblages. If, as is commonly assumed, oxygen ions are the largest ions in the pyroxene lattice, oxygen vacancies could have a more important influence on chemical diffusion rates, especially the Ca diffusion rate, than on electrical conductivities. Therefore, bulk chemical diffusion in pyroxenes would be favored by reducing conditions, not oxidizing conditions as is commonly assumed.

Introduction

When Huebner et al. (1979) measured the electrical conductivity of orthopyroxene as a function of temperature, composition, orientation, and f_{O_2}, the resulting measurements were not sufficiently systematic to be interpreted in terms of the activation energies and mechanisms needed to model pyroxenes that exist under different conditions. Huebner et al. went on to stress that differences in the states of aggregation might bring about uncertainties in applying laboratory measurements on single crystals to real rocks. The 1982 Chapman Conference on Point Defects (Schock, 1985) emphasized the importance of considering point defects when trying to interpret electrical and mechanical properties measured in the laboratory. Recently, we have encountered similar uncertainties when applying laboratory measurements of chemical diffusion rates to natural assemblages. To address these un-

* Present address: Department of Geosciences, 204 Deike Building, Pennsylvania State University, University Park, Pennsylvania 16802, U.S.A.

0003–004X/88/1112–1235$02.00

certainties, we chose to return to electrical measurement techniques because they are a fast, yet accurate, method for deducing defect structures (Tuller, 1985). We chose initially to focus on relatively pure diopside for three reasons. (1) Augite is an important mineral in mafic rocks and the mantle, where it contributes to observed electromagnetic sounding profiles and has undergone transformations involving chemical diffusion. (2) Diopside, the principal end member of most augites, is chemically simple, thereby reducing the number of compositional variables. (3) There is no unambiguous set of electrical conductivity measurements for this phase or for any other pyroxene. In this first report we limit ourselves to measurements on the diopside single crystals that will be used to synthesize aggregates for future studies. In future reports, we expect to discuss how changes in the state of aggregation and the cation ratios will change the measured conductivities, enabling us to compare data on single crystals and polycrystalline aggregates and to extract bulk conductivity data from aggregates prepared to desired compositions. This long-range intention influenced our choice of measurement technique.

Previous work

Reports in the literature present an ambiguous "picture" of pyroxene electrical-conductivity values (data that can be used to quantify geophysical models that use natural compositions, temperatures, pressures, and redox states). A review of previous measurements suggests that the conductivity measurements themselves are precise; rather, the ambiguity is probably caused by subtle changes in composition or by differences in the state of aggregation within the sample cell. The following summary will illustrate some of the uncertainties in past efforts and thereby provide a rationale for the design of our experiments.

Much early work dealt with crystals that contained inclusions of a second phase (commonly talc). For instance, Duba et al. (1973) measured three orthopyroxene single crystals at 525 to 1009 °C, controlled oxygen fugacity, 1-bar pressure, and 1592 Hz. Two of the samples contained talc (A. Duba, pers. comm.), which should have dehydrated in this temperature range and probably caused the anomalously large and unstable conductivity values observed when the samples were first heated. Gem-quality orthopyroxene [$Na_3Ca_{23}Mn_2Mg_{1786}Fe_{156}Ni_1Cr_6Ti_4Al_{24}Si_{1988}O_{6000}$], the third sample, had no talc inclusions and behaved stably. Although it had an intermediate value of Fe/(Mg + Fe) and higher concentrations of minor components, the gem-quality orthopyroxene was less conductive than the two other pyroxenes, $Na_2Ca_3Mn_3Mg_{1873}Fe_{150}Cr_4Ti_1Al_8Si_{1975}O_{6000}$ and $Ca_{13}Mg_{1708}Fe_{278}Ni_1Al_7Si_{1995}O_{6000}$. Measured activation energies at constant values of f_{O_2} were in the range 1.2–1.9 eV with a slight tendency for higher values at temperatures greater than 900 °C. At 1000 °C, the slope of $\partial(\log \sigma)/\partial(\log f_{O_2})$ varied from $1/12$ to $-1/12$, where σ is electrical conductivity.

Duba et al. (1976) subsequently measured orthopyroxene from Bamble, Norway; we identified talc in this sample and determined the bulk composition to be remarkably devoid of Al and Cr, $Na_3Ca_{11}Mn_1Mg_{1655}Fe_{288}Ti_2Al_4Si_{2014}O_{6000}$. At 1000 °C and $\log f_{O_2} = -9.5$ (f_{O_2} in bars), initial values were again anomalously conductive and unstable, presumably because of dehydration of the talc. Subsequent measurements were stable. At 1000 °C and $\log f_{O_2}$ of -1 to -16, the slope $\partial(\log \sigma)/\partial(\log f_{O_2})$ was $-1/16$. At 5-kbar pressure and $\log f_{O_2}$ approximately -12, the results were complicated by (presumably) dehydration and melting. The apparent activation energies were 1.0 eV at <1250 °C and 1.8 eV at >1250 °C. The conductivity was greater at 5 kbar than at 1 bar.

Dvorak and Schloessin (1973), in an investigation designed to reveal conduction mechanisms, also measured an orthopyroxene from Bamble, Norway. We have found two compositions (Mg:Fe = 96:3 and 86:13) of orthopyroxene from this locality, each with included talc (and one with magnetite). Unfortunately, Dvorak and Schloessin failed to identify the composition of their pyroxene, worked at a difficult experimental range of pressure (24–56 kbar) and low temperature, and neither measured nor defined the redox state (f_{O_2}) of the orthopyroxene. Measured values of the activation energy ranged from 0.45 to 0.65 eV, distinctly lower than most other values. On the basis of the variation with pressure and temperature, the activation energy could be resolved into two terms. The dominant energy term was associated with increasing the number of charge carriers; only 0.06–0.08 eV was attributed to migration.

Will et al. (1979) measured the conductivity of synthetic Fe-free orthoenstatite ($Mg_2Si_2O_6$) aggregates at 10 kbar and 1600 Hz, using quartz to buffer the silica activity or forsterite to buffer the MgO activity. No attempt was made to distinguish the bulk component from any grain-boundary component of the measured conductivity. On the assumption that the conductivity would be independent of f_{O_2}, they made no attempt to control or measure f_{O_2}. At 600 °C the measured conductivity of enstatite in equilibrium with quartz was slightly greater than for enstatite in equilibrium with forsterite. With increasing temperature, the differences in conductivity declined until, at 1000 °C, the conductivities were equal. The measured activation energies were 1.11 eV for enstatite in equilibrium with quartz and 1.25 eV for enstatite in equilibrium with forsterite. The usefulness of these conductivity values must be regarded as uncertain because of the uncertainty in prevailing f_{O_2}.

In a similar study, Voigt et al. (1979) searched for systematic variation between the conductivity of synthetic orthopyroxene aggregates and pressure or Fe/(Mg + Fe). Conductivity regularly increased with increasing Fe/(Mg + Fe) over the complete range of solid solution. Over the range Fe/(Mg + Fe) = 0.0 to 0.2, an increase in pressure from 10 to 20 kbar decreased the conductivity and increased the activation energy. At Fe/(Mg + Fe) = 0.5, the effect of pressure was small. A surprising feature of

these results is that conductivities of the Fe-rich pyroxenes at temperatures of 900 °C, below that of the pyroxene solidus, exceed the conductivities expected of basaltic melts, whereas we would have expected the silicate melts to be more conductive than the crystalline silicates. The decrease in conductivity of polycrystalline aggregates with pressure contrasts in behavior to the increase found in single crystals by Duba et al. (1976). Perhaps, in the case of the aggregate, the decrease in conductivity is due to a closing of grain boundaries with pressure, rather than being a bulk property of the pyroxene. Leakage paths across the high-pressure assemble and the inability of controlling oxygen fugacity are additional factors to be considered.

Huebner et al. (1979) questioned the use of compositionally pure natural and synthetic pyroxenes as analogues of pyroxenes that contain significant concentrations of trivalent elements, as is the case in many natural assemblages. By comparing measurements of three gem-quality orthopyroxene crystals having similar Fe/(Mg + Fe), the least pure with composition $Na_2Ca_7Mn_6Mg_{1622}Ni_9Fe_{311}Cr_{15}Al_{77}Si_{1952}O_{6000}$ (reanalyzed by us), they demonstrated that increased Al^{3+} and Cr^{3+} content was associated with increased conductivity. They observed no dependence of conductivity on f_{O_2} or frequency (50 Hz to 10 kHz). Despite use of gem-quality crystals that contained no inclusions, the results were unsystematic with respect to crystallographic orientation. The authors chose not to tabulate activation energies that might be used for unwarranted extrapolations. Approximate values of 1.3 eV at >1000 °C and 1.0 eV at <1000 °C can be estimated from their Figure 7, suggesting a change in conduction mechanism at about 1000 °C. Duba et al. (1979) measured very aluminous orthopyroxene ($Na_8Ca_{60}Mn_7Mg_{1376}Fe^{2+}_{409}Fe^{3+}_{31}Cr_1Al_{290}Ti_{14}Si_{1818}O_{6000}$) and confirmed the trend of increasing conductivity with increasing trivalent-element content. They also noted a break in the slope of conductivity at about 900 °C; from their Figure 1 we estimate a high-temperature activation energy of 1.2 eV and a low-temperature value of 0.8 eV, similar to energies estimated from Huebner et al. (1979). In contrast, the pure polycrystalline orthoenstatite of Will et al. (1979) at 1000 °C and 10 kbar was *more* conducting than these impure pyroxenes and at 700 °C had conductivity equal to the most conducting impure pyroxenes.

Hinze et al. (1981) also found that natural aluminous enstatite aggregate ($Na_{12}Ca_{47}Mn_4Mg_{1682}Fe_{185}Cr_{13}Ti_6Al_{256}Si_{1858}O_{6000}$) was *less* conducting than synthetic aggregate with comparable Fe/(Mg + Fe) but no additional components. Again, no attempt was made to distinguish bulk and grain-boundary components of the conductivity. The activation energy was 1.0–1.1 eV, but the temperature range (<850 °C) was not sufficient to reveal a change in slope. Clinopyroxene aggregate behaved differently. Natural augite of composition $Na_3Ca_{530}Mn_6Mg_{1015}Fe_{121}Cr_{11}Ti_{20}Al_{566}Si_{1711}O_{6000}$, thermodynamically buffered by the olivine-orthopyroxene assemblage in which it occurred, was an order of magnitude more conducting than synthetic $CaMgSi_2O_6$ at 10 kbar (and unknown f_{O_2}). Hinze et al. (1981, p. 250) attributed the enhanced conductivity to the Fe content of natural diopside; we would have attributed a significant role to the trivalent elements Al and Cr. The activation energies are distinct: 0.4 eV for the natural and 1.3 eV for the synthetic diopside. The value of 0.4 eV is matched only by the values of Dvorak and Schloessin (1973) for Bamble orthopyroxene at high pressures and low temperatures and by the values of Voigt et al. (1979) for synthetic $FeSiO_3$ at 20 kbar.

Most recently, Parkhomenko (1982) reviewed conductivities obtained from six contrasting compositions of pyroxene. At 300 °C, a temperature at which she expected that extrinsic conductivity caused by impurities would predominate, diopside and enstatite were poor conductors (10^{-7} to 10^{-8} S/m) but hedenbergite and acmite were relatively good conductors (10^{-3} S/m). Activation energies, calculated from plotted data, ranged from 0.2 to 0.7 eV. Without chemical analyses or knowledge of the structural state, it is probably unwarranted to conclude that increased conductivity is caused by alkalis or Fe. At 1000 °C, conductivities ranged from 10^{-4} to 10^{-2} S/m (enstatite, diopside, spodumene) to 1 to 10 S/m (jadeite, hedenbergite, acmite). Activation energies of 2.7, 0.7, and 4.4 eV, respectively, are reported for this latter group. The highest conductivity values may be due to decomposition or melting, making uncertain the significance of the reported activation energies. This systematic approach was extended to measurements at 1 to 20 kbar, showing that conductivity increased with the sum of alkalis, FeO, and Fe_2O_3 and with pressure. In no case, however, is enough information given about a sample, the measurement technique, or the conditions of measurement to compare the magnitude of a measurement with that determined in another laboratory.

Despite much effort using orthopyroxene and two studies using Ca-rich clinopyroxenes, it is difficult to place the conductivity measurements into a systematic framework. Conductivity does not change simply with crystallographic orientation, Fe/(Mg + Fe), trivalent-element content, pressure, or state of aggregation (Fig. 1). There appear to be two families of activation energies, <0.8 and >1.0 eV, with the lesser values occurring at low temperature. Some conductivities appear to depend upon the furnace f_{O_2}, but others do not. It is clear that resolution of these ambiguities will require, at a minimum, knowledge of the chemistry and structural state of the substance being measured, characterization of a sufficient quantity of material that measurements can be made on different states of aggregation at different physical conditions, the ability to vary cation/cation and cation/anion ratios, and the control and measurement of oxygen fugacity during the measurements. In this paper we only begin to address these issues, limiting ourselves to (1) single crystals, (2) minimal composition variation, and (3) 1-bar pressure with the intent of defining how conductivity and conductivity mechanisms vary with temperature, crystallographic orientation, and f_{O_2}. In future work, we will study an isotropic aggregate of identical bulk composition, using

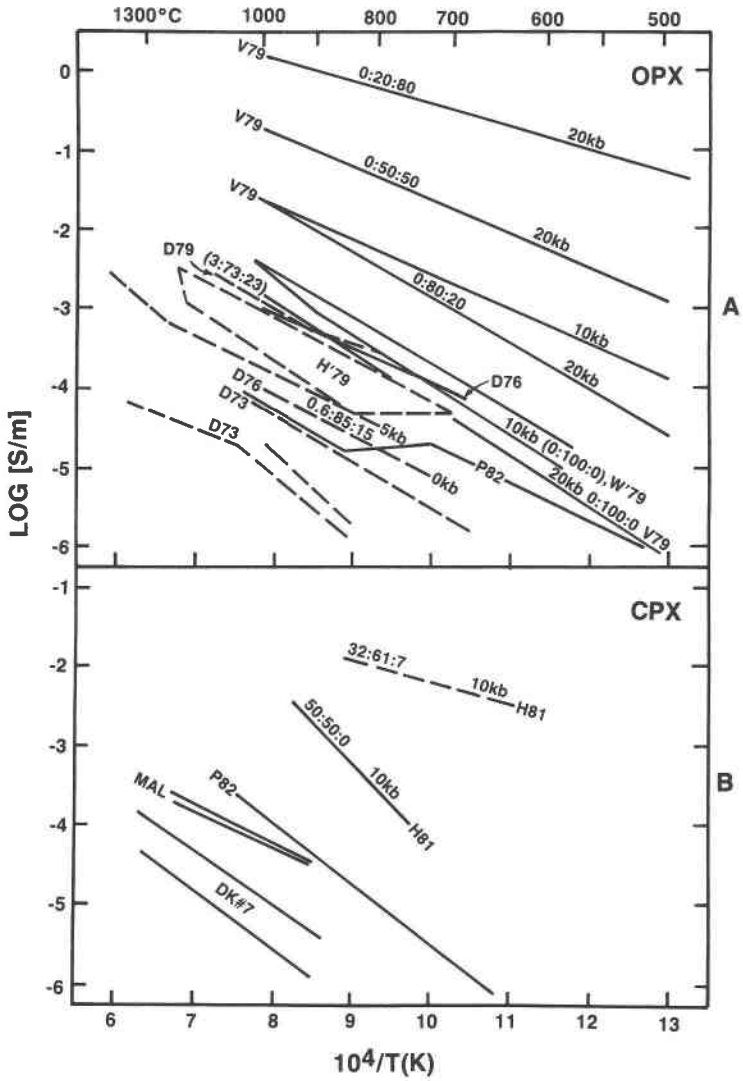

Fig. 1. Summary of electrical conductivity measurements of pyroxenes discussed in text. Solid lines represent synthetic pyroxenes that contain no impurities such as trivalent elements; dashed lines represent natural, impure samples. Compositions are indicated as atomic proportions of Ca:Mg:Fe. Total pressure is 1 bar unless indicated. (**A**) Orthopyroxene; (**B**) clinopyroxene. Sources of data: D73 (Duba et al., 1973), D76 (Duba et al., 1976), V79 (Voigt et al., 1979), W'79 (Will et al., 1979), H'79 (Huebner et al., 1979), D79 (Duba et al., 1979), H81 (Hinze et al., 1981), P82 (Parkhomenko, 1982). DK7 and MAL represent conductivity ranges of the two diopsides reported in this study. The results of Dvorak and Schloessin (1973) were collected at low temperatures (293–507 K) and are not shown.

changes in the frequency, temperature, and f_{O_2} responses of conductivity to distinguish the components of grain-boundary and volume conduction. In this manner, we will explore the relationship between measurements made on single crystals and on aggregates. Finally, we will investigate the effects of varying the cation ratios (both proportions of elemental constituents and deviations from stoichiometry) of synthetic aggregates having compositions that cannot be obtained in natural single crystals.

Characterization of diopside

Crystal DK7 is one of several hundred 1- to 3-cm-sized diopside crystals collected from a vug near De Kalb, New York for Wards, Inc.,[1] and acquired at the suggestion of one of us (J.S.H.) by the U.S. National Museum of Natural History, Washington, D.C. We initially selected six crystals (DK1–DK6); the USNMNH subsequently assigned acquisition numbers R18682–R18684 to the lot. We later obtained three more crystals (DK7–DK9) from split R18682. These crystals are very pale green; 0.7- to 1.5-mm-thick plates are colorless. White, clay-like material (talc) adheres to some surfaces; cracks and fluid inclusions make some parts of the crystals cloudy. For this first report, we used only the clear, gem-quality portions of crystal DK7.

We also used green diopside from Malacacheta, Brazil, removed from a lot that was subsequently assigned USNMNH acquisition numbers 125990 and 127104. Diopside from Malacacheta is intense green, even in 1-mm plates, and shows "oscillatory" zoning in color and slight heterogeneity in Fe/Mg ratio. The cracks appear unfilled, yet thin plates of the material remain intact.

Microprobe analyses of the crystals were performed by

[1] Use of trade names and names of suppliers of materials and equipment is for descriptive purposes only and does not imply endorsement by the U.S. Geological Survey.

TABLE 1A. Chemical analyses of diopside

	DK7			Avg DK1–9	PXKA***		MAL	
	Unheated	Heat*	Heat**	Unheated	Found	Expected	Unheated	Heated†
				Microprobe (wt%)				
SiO_2	55.64(25)	55.67(35)	56.06	55.58(31)	50.61(53)	50.73	54.59(28)	54.60(22)
P_2O_5	0.01(02)	0.00(00)	0.00	0.01(02)	0.01(01)	n.a.	0.00(00)	0.00(00)
Al_2O_3	0.54(04)	0.56(19)	0.58	0.52(07)	8.78(21)	8.73	0.66(18)	1.03(03)
TiO_2	0.02(01)	0.02(00)	0.01	0.01(01)	0.77(02)	0.74	0.01(00)	0.01(00)
Cr_2O_3	0.00(00)	0.00(00)	0.00	0.00(00)	0.15(01)		0.17(04)	0.15(03)
MgO	17.90(14)	17.84(12)	18.01	17.99(14)	16.61(19)	16.65	15.92(14)	16.18(28)
Fe††	0.88(04)	0.88(02)	0.92	0.81(07)	6.36(10)	6.34	4.14(12)	3.74(07)
NiO	0.01(01)	0.01(01)	0.00	0.01(02)	0.03(01)		0.04(02)	0.06(01)
MnO	0.05(00)	0.06(01)	0.06	0.06(01)	0.13(01)	0.13	0.13(01)	0.12(00)
CaO	24.83(16)	24.72(10)	24.91	24.86(14)	15.41(26)	15.82	24.48(11)	24.50(14)
ZnO	0.01(01)	0.02(02)	0.02	0.02(01)	0.02(02)		0.02(02)	0.01(01)
Na_2O	0.40(02)	0.40(01)	0.43	0.38(04)	1.31(03)	1.27	0.21(02)	0.27(01)
Subtotal	100.30(44)	100.18(40)	100.98	100.26(38)	100.20(90)	100.41	100.37(66)	100.66(32)
Analyses	6	4	2	25	18		4	4
Points	46	32	16	186	67		32	32
				Semiquantitative emission spectrographic analyses (ppm)†††				
ZrO_2	24			9–39			14	
TiO_2	300			160–380			230	
CeO_2	<43			<43			66	
P_2O_5	<1550			<1550			<1550	
V_2O_5	41			41–59			66	
Sc_2O_3	3			3–5			15	
B_2O_3	110			64–110‡			n.a.	
Cr_2O_3	3			2–14		1200	1750	
Dy_2O_3	<25			<25			25	
Er_2O_3	<1			<5			18	
La_2O_3	<12			<12–16			<12	
Y_2O_3	4			3–6			7	
NiO	8			7–13		460	600	
CoO	<2			<2–13			38	
MnO	340			340–1550			2700	
CuO	8			3–16			6	
GeO	<7			<7			7	
PbO	<7			<7–18			18	
SrO	21			16–33			70	
ZnO	110			<12–120		37	210	
K_2O	<820			<820–1110			<820	
Li_2O	<150			<150–<250			215	
Total‡‡	100.32			100.31		100.58	100.50	

Note: n.a. = not analyzed. f_{O_2} in bars.

* 1000 °C, log $f_{O_2} = -17.47$.

** 1200 °C, log $f_{O_2} = -7.65$.

*** Sources of data are summarized in Huebner and Woodruff (1985).

† 900 °C, log $f_{O_2} = -17.63$.

†† All Fe assumed to be divalent.

††† J. D. Fletcher, U.S. Geological Survey, analyst. Jobs BN69 and BV07. Originally reported as element ppm.

‡ Only DK7–9 were analyzed.

‡‡ In calculating totals, values "<" assumed zero. Except for PXKA, totals were calculated using means of microprobe and emission spectrographic results for TiO_2, Cr_2O_3, NiO, MnO, and ZnO.

standard analytical procedures using the reduction scheme of Bence and Albee (1968). Primary standards were silicates and an oxide, evaluated by Huebner and Woodruff (1985) and used as follows: AMKH (Al, Ti); FSBO (P); OLNI (Ni); OXTB (Cr); PXBK (Zn); PXEN (Mg); PXHD (Fe, Mn); PXKA (Na); and PXPS (Si, Ca). Backgrounds were obtained by interpolation, based on the mean atomic number of the unknown, between the count rates obtained on OXQZ or OXPE at low Z and OXNC or OXVA at high Z. We used a focused 15-kV electron beam, a nominal 15-nA sample current, and a count time of 30 to 90 s for peak measurements and 120 s for backgrounds. A pyroxene analysis was calculated from X-ray count data obtained from four to eight consecutive spot analyses. We report the mean of pyroxene analyses made on two or more operating shifts (Table 1A), thereby "averaging out" the shift-to-shift scatter that was most evident in values for Si. For comparison, the mean of replicate analyses of working standard PXKA and the expected value (classical mineral analysis) are given. The agreement is good for all major elements execpt Ca. Long-term monitoring of the CaO contents of a suite of working standards and use of a substitute primary standard (PXP1) for Ca (and Si) suggests that the assumed Ca value of the working standard is too low. Thus, no adjustment to the CaO value of the De Kalb diopsides was applied before calculating nominal formula units (Table 1B) from the chemical analyses (Table 1A).

TABLE 1B. Nominal formula units per 40000 cations, analyzed diopside

Position	Cation	DK7			DK1–9	MAL	
		Unheated	Heated (001) plate*	Heated (100) plate**	Unheated	Unheated	Heated (010) plate†
T	Si	20020	20056	19989	19989	19911	19803
	P^{5+}	3	3	3	3		
	V^{5+}	1	1	1	1	2	2
	B	7	7	7	5		
	Al				2	87	195
ΣT		20031	20067	20000	20000	20000	20000
M(1)	Ti^{4+}	7	7	5	5	4	4
	Al	229	238	99	218	197	244
	Cr^{3+}					50	47
	Ni	2	2	0	16	15	17
	Co^{2+}					1	1
	Fe^{2+}	162	173	219	117	1263	1136
	Mg	9600	9580	9677	9644	8470	8551
ΣM(1)		10000	10000	10000	10000	10000	10000
M(2)	Fe^{2+}	103	92	127	127	187	192
	Mn^{2+}	13	16	24	24	62	60
	Ce^{4+}					1	1
	Sr			1	1	1	1
	Zn	3	4	3	3	4	4
	Ca	9572	9542	9579	9579	9567	9520
	Na	279	279	265	265	146	190
	Li					32	31
ΣM(2)		9970	9933	9997	9999	10000	9999
Oxygens		60010	60050	59830	59980	60000	59940

Note: Footnotes are in Table 1a.

Each crystal was also analyzed by semiquantitative emission spectrographic (DC arc) techniques; the results are also summarized in Table 1A. As a rule-of-thumb, these results have an uncertainty of ±50% and give us confidence in microprobe determinations at the level of <0.1% (1000 ppm).

Chemical analyses were converted to nominal site occupancies based on 40000 cations (Table 1B), and charge balance was assumed to be maintained by oxygen ions (divalent anions). The cation to oxygen ratios are very close to that of ideal pyroxene (4:6) and suggest that Fe^{3+} is not present. However, without a direct determination of the anions or of the oxidation states of the polyvalent elements, we cannot conclude that these pyroxenes are perfectly stoichiometric. Crystal DK7 has almost end-member $CaMgSi_2O_6$ composition with Fe/(Mg + Fe) = 0.027. The fact that the chemistry of DK7 cannot be distinguished from the average of the nine DK diopside crystals suggests that the inherently inaccurate minor- and trace-element analyses are at least precise (i.e., consistent). Within limits of analytical error, the nominal site occupancies suggest that tetrahedral (T), octahedral (M1), and 6- to 8-fold coordinated M(2) sites are fully occupied with cations of appropriate size. In particular, there is no evidence for small interstitials such as Si. If the M(2) site of the De Kalb diopsides is fully occupied with Ca, Na, Zn, and Sr [which are too large to fit into the M(1) or T positions], De Kalb diopsides contain no significant concentrations of octahedral vacancies. The chemistry of the Malacheta diopside is similar except for its greater Fe/(Mg + Fe) value of 0.127.

Unit-cell dimensions (Table 2) were determined by

TABLE 2. Unit-cell dimensions and densities of diopsides

	DK7				DK1–9	MAL
	Unheated	DK7(001)-2	DK7(010)-3	DK7(100)-2	Average	MAL(100)
a (Å)	9.738(2)	9.743(1)		9.744(1)	9.742(3)	
b (Å)	8.921(2)	8.920(1)		8.922(1)	8.920(2)	
c (Å)	5.249(1)	5.248(1)		5.252(1)	5.252(3)	
β (°)	105.84(2)	105.85(2)		105.85(1)	105.85(2)	
V(Å^3)	439.7(1)	438.7(1)		439.2(1)	439.1(2)	
ρ_{calc}	3.275	3.296		3.280	3.279	
T (°C)	unheated	1001	1200	1200	unheated	unheated
log f_{O_2} (f_{O_2} in bars)		−17.47	−12.00	−7.66		
ρ_{obs}	3.270(9)	3.271(4)	3.275(2)	3.290(9)	3.263(17)	3.315(3)
No. of ρ observations	17	8	5	8	9	4
$\rho_{obs} - \rho_{calc}$	−0.004	−0.025		+0.008	−0.016	
Condition	?	reduced	reduced	oxidized	?	?

X-ray powder diffractometry using BaF_2 internal standard [a_0 = 6.1971(1) Å] and an automated method similar to that described by Huebner and Papike (1970) except for the use of magnetic tape-recording medium instead of punched paper tape. Densities of regularly shaped pyroxene fragments, each approximately 25 mg in weight, were determined by immersion in carbon tetrachloride, using a microbalance. Densities determined by immersion are inherently imprecise; nevertheless, measured densities of unheated DK and MAL diopsides are within 0.7% of the values calculated from the composition and unit-cell dimensions, assuming 16 cations and 24 oxygens (40 atoms) per unit cell (Table 2). Because the substitution for oxygen of anions with different atomic weights would change the density, the agreement indicates that an oxygen-based formula unit is appropriate.

Natural diopside crystals such as these deserve greater attention from geophysicists. We suspect that the De Kalb crystals are more homogeneous and stoichiometric than could be achieved by laboratory growth from a silicate melt of even pure diopside bulk composition. This is because diopside melts incongruently (and nonstoichiometrically) to a melt enriched in SiO_2 and $CaSiO_3$ components and a residual pyroxene enriched in Mg_2SiO_4 and $Mg_2Si_2O_6$ components (Kushiro, 1972). Pyroxene crystals grown from a flux will, in addition, most likely contain components of the flux in solid solution. Our De Kalb pyroxenes suffer none of these uncertainties.

Experimental technique and uncertainties

Oriented plates of each diopside sample were gently ground and polished, finishing with 0.05-μm alumina, then cleaned in an ultrasonic bath. The sides were parallel to within 0.03 mm. Most plates were briefly milled with Ar plasma, then coated with a thin layer of evaporated Pt. Thickness (l) was measured to within 0.02 mm, and the uncertainty in area (A) was <5% (sum of measurement area and lateral slippage of Pt foil). One half of the symmetrical sample cell consisted of an oriented diopside plate with nominal 1-cm² area, Pt paint, 0.13-mm Pt foil cut to the shape of the diopside plate, Pt paint, Ir plate (14.7 mm in diameter by 0.36 mm thick), and supporting rods of dense alumina (Vistal, supplied by Coors Porcelain Company). Uncertainties in the geometry of the sample cell are less than 5%. The reversibility of our data and electron-microprobe analyses of heated plates suggest that systematic loss of Fe to the electrodes was not a problem.

Our furnace configuration is vertical with an alumina muffle tube of 44-mm inner diameter. The temperature and oxygen fugacity were maintained constant and measured using the nonautomated techniques described by Huebner (1987). Pt-$Pt_{90}Rh_{10}$ thermocouple wire was calibrated against the melting points of diopside and gold; the entire measurement circuit was calibrated against the ice point and the gold melting point. The oxygen-fugacity sensor was placed beside the sample cell; the temperature gradient across the sample cell and sensor was less than 2 °C. Measured temperatures are believed accurate to ±1.5 °C. The gas flow rate entering the furnace was 1.67 cm³/s to give liner flow rates of 1.2 mm/s at the bottom of the furnace (cold) and 6.7 mm/s (estimated) past the cell and sensor at 1200 °C. These flow rates are much slower than is generally recommended. At high temperatures, measured f_{O_2} agreed with that calculated (Deines et al., 1974) from the mixing ratio of CO and CO_2 to within 0.10 log unit; at lower temperatures, the measured f_{O_2} was less than calculated, although not by as much as might be expected at higher rates of flow (Huebner, 1975). Over a wide range of f_{O_2} values, we saw no evidence that the oxygen-fugacity sensor (type $SIRO_2$ from Ceramic Oxide Fabricators) developed a component of electronic conduction.

Impedance spectra were obtained with a model 273 potentiostat and model 5208 two-channel lock-in amplifier, manufactured by EG&G Princeton Applied Research, and the manufacturer's "turn-key" software that uses the composite-waveform (FFT) method at <11 Hz and the lock-in method at >5 Hz. The waveform amplitude across the cell was 5–100 mV and decreased with increasing frequency. Measured impedances of Teflon and silica glass exceeded 10^{10} Ω at room temperature, and the impedance of single-crystal alumina [001] exceeded $10^{6.5}$ Ω at 1200 °C, $10^{7.0}$ Ω at 1000 °C, and $10^{8.0}$ Ω at 800 °C. These values, which reflect the combination of bulk and leakage conductances, provide minimum resistances for leakage paths across the cell. In comparison, the measured impedances of all diopside plates but DK7(010)-3 at relatively high f_{O_2} values were smaller than that of the alumina plate. We will see later that the behavior of this diopside plate, although less conductive than other diopside plates, suggests measurement of bulk conductivity rather than leakage. Addition of a series capacitor to the measurement circuit caused the impedance to decrease to ~1 Ω at high frequency, demonstrating the absence of a series resistance in the measurement circuit. Reported impedances are those at which the phase (θ, the angle by which the change in current lags behind the change in voltage) is approximately equal to zero. Commonly, we find this maximum value of θ at 10–100 Hz. Reference spectra (Fig. 2), collected with networks of known components chosen to stimulate the highest- and lowest-temperature measurements and mounted in place of the sample cell, always yielded FFT and lock-in measurements within 0.05 log σ unit of the expected values, commonly within 0.01 log σ unit. Further interpretation of the spectra will be discussed in a subsequent paper in which we identify the contribution that grain boundaries make to conduction.

Measured impedance (Z) was first converted to conductance ($1/Z$) and then to specific conductance (σ, commonly called conductivity with units of siemens per meter) using $\sigma = (1/Z)(l/A)$, where l is the thickness and A the area of the sample. Values of the geometric factor, GF = l/A, ranged from 8.7 to 55 m⁻¹ (Table 3). Thus the absolute values of the conductances (impedances) measured by the equipment were less (greater) than the reported conductivities (resistivities). Values of log σ were plotted as iso-

Table 2.—*Continued*

MAL			
MAL(010)-1		MAL(010)-1	MAL(100)-1
9.751(2)	9.754(2)	9.760(1)	9.750(1)
8.929(2)	8.924(2)	8.936(1)	8.926(1)
5.2510(15)	5.253(1)	5.251(1)	5.252(2)
105.78(2)	105.81(2)	105.78(2)	105.77(2)
440.0(0)	440.0(1)	440.7(1)	439.9(1)
3.334		3.320	
unheated		900	1100
		−17.61	−9.28
3.311(9)		3.276(3)	3.303(3)
9		6	5
−0.028		−0.045	
?		reduced	oxidized

TABLE 3. Measured conductivities (σ in siemens per meter), lock-in technique

Date	Time	Duration (h)	T (°C)	log f_{O_2}	log σ	Residual*
36.3-MΩ resistor, expected log σ = −7.556 to −7.564						
4/01					−7.56	
10-kΩ resistor, expected log σ = −3.996 to −4.004						
4/07	16:00				−4.00	
DK7(100)-2, GF = 9.68 m^{-1}, l_i = 0.068 cm, l_i = 0.068 cm						
3/30	06:55	87.3	1200	−8.82	−4.40	−0.032
	10:21	90.7	1200	−8.50	−4.43	−0.006
	13:23	0.7	1300	−7.22	−4.13	0.053
	15:39	2.9	1300	−7.22	−4.15	0.033
3/31	9:45	1.8	1200	−8.48	−4.45	−0.022
	11:27	0.9	1300	−8.48	−3.95	0.009
	13:29	1.1	1100	−8.50	−5.0	−0.040
	15:35	1.2	1000	−8.47	−5.68	−0.093
4/01	12:55	3.7	1300	−6.99	−4.17	0.054
	15:41	1.9	1200	−7.00	−4.63	0.060
4/02	9:30	17.0	1100	−7.05	−5.30	−0.082
	11:52	1.2	1000	−7.58	−5.80	−0.055
	15:44	3.0	1300	−6.00	−4.30	0.100
4/03	8:54	1.5	1200	−6.02	−4.86	0.004
	10:17	0.7	1100	−6.02	−5.43	−0.029
	13:21	1.8	1300	−5.04	−4.36	
	15:43	1.6	1202	−5.01	−4.91	0.124
4/04	17:05	6.0	1298	−3.91	−4.43	
4/05	16:02	6.1	1300	−3.23	−4.41	
4/06	9:42	2.2	1200	−3.47	−5.0	
	13:33	2.7	1100	−3.45	−5.45	
	15:13	0.7	1000	−3.42	−5.9	
4/07	8:10	16.0	1300	−10.93	−3.6	−0.076
	12:00	2.6	1300	−11.92	−3.5	
	14:56	6.8	1200	−11.89	−3.86	−0.038
4/08	8:30	18.8	1200	−11.90	−3.89	−0.075
	11:06	1.5	1100	−11.97	−4.30	0.044
	13:01	1.1	1000	−12.10	−4.78	0.162
	15:07	0.7	1300	−12.79	−3.53	
	16:10	5.9	1201	−12.94	−3.83	
4/09	10:07	1.6	1100	−12.98	−4.20	−0.035
	13:46	2.0	1000	−13.04	−4.67	0.105
	15:55	6.8	1200	−14.06	−3.83	
4/10	11:01	2.9	1100	−13.98	−4.16	
	14:15	2.1	1000	−13.98	−4.59	0.018
	16:02	6.1	1198	−14.63	−3.92	
4/11	14:39	>2.7	1000	−17.78	−4.57	
4/13	8:40	16.0	1200	−7.65	−4.66	−0.085
	12:13	19.9	1200	−7.66	−4.67	−0.097
DK7(010)-1, GF = 12.59 m^{-1}, l_i = 0.075, l_i = 0.075						
9/12			1200	− 8.46	−4.93	0.0013
9/15			1300	−7.32	−4.51	
9/16			1102	−9.80	−5.34	−0.0560
			1002	−11.33	−5.75	−0.0452
			1100	−10.56		
9/17			1300	−11.10	−4.23	−0.0056
			1197	−12.42	−4.57	−0.0298
			1108	−13.72	−4.85	
9/18			1100	−13.86	−4.90	
DK7(010)-2, GF = 18.42 m^{-1}, l_i = 0.106 cm, l_i = 0.107 cm						
4/14	14:38	2.0	1200	−8.46	−4.20	
	15:46	6.0	1200	−8.46	−4.70	
4/16	8:22	55.0	1200	−8.46	−4.96	
4/17	16:17	85.0	1200	−8.46	−4.96	−0.0287
4/20	16:05	6.1	1100	−9.15	−5.47	−0.1088
4/21	11:54	2.2	1000	−9.00	−5.92	
	16:03	2.4	900	−9.13	−6.32	
4/22	12:45	3.0	1300	−7.83	−3.89	
	14:51	5.0	1300	−7.83	−3.91	
	16:19	10.0	1299	−7.84	−4.08	
4/23	9:02	23.0	1299	−7.81	−4.12	
	14:55	31.0	1299	−7.81	−4.17	
2.42-MΩ resistor, expected log σ = −6.384						
4/24					−6.35	
Measurements of DK7(010)-2 conductivity resumed						
4/24	6:45	13.1	1300	−7.15	−4.33	
	11:30	17.9	1300	−7.15	−4.36	
	15:43	22.1	1300	−7.15	−4.39	
4/25	10:36	42.0	1300	−7.15	−4.41	
4/27	15:09	4.4	1300	−5.66	−4.50	
	15:47	13.3	1202	−6.92	−5.03	
4/28	16:43	38.3	1201	−6.94	−5.04	
4/29	15:48	7.0	1100	−8.41	−5.5	
4/30	8:58	1.5	1000	−10.11	−5.92	−0.0779
	13:46	1.1	900	−12.09	−6.30	0.0173
	15:39	9.0	1300	−3.36	−4.51	
5/01	10:16	2.0	1200	−3.40	−5.02	
	12:01	1.0	1002	−3.36	−5.95	
	15:42	10.8	800	−3.22	−6.70	
5/04	13:27	3.3	1300	−8.93	−4.30	
	15:51	11.7	1300	−8.92	−4.30	0.1474
5/05	10:11	2.0	1200	−9.02	−4.8	0.0740
	13:15	2.0	1300	−9.90	−4.24	
	16:05	10.0	1300	−9.90	−4.23	0.1172
5/06	15:17	3.0	1200	−9.98	−4.77	
5/07	12:00	21.3	1200	−9.98	−4.79	−0.0142
	16:25	10.7	1100	−10.08	−5.32	−0.0539
5/08	15:45	10.0	1200	−13.85	−4.54	
5/11	8:10	70.7	1200	−13.84	−4.50	
2.15-MΩ resistor, expected log σ = −6.332						
5/11					−6.334	
Measurements of DK7(010)-2 resumed						
5/18	9:00	70.0	1100	−15.10	−4.92	
	12:40	1.8	1000	−16.79	−5.36	
	14:57	1.4	900	−16.91	−5.89	
2.42-MΩ resistor, expected log σ = −6.384						
5/21					−6.385	
Measurements of DK7(010)-2 resumed						
5/21	15:45	72.0	1200	−12.66	−4.53	−0.0284
5/22	16:30	32.3	1300	−12.81	−4.10	−0.0506
5/23	19:33	8.3	1206	−12.57	−4.57	−0.0871
5/25	17:08	8.4	1000	−13.00	−5.52	0.0264
5/26	9:58	2.0	900	−13.09	−6.10	0.1150
	15:50	5.0	1200	−14.08	−4.52	
5/27	8:29	21.3	1200	−14.25	−4.54	
	13:03	3.3	1100	−13.91	−4.96	
	14:42	0.4	1000	−13.97	−5.46	
	16:16	9.0	902	−13.96	−6.07	0.0413
5/28	12:00	3.3	1100	−12.40	−5.00	0.0287
	16:13	11.3	1300	−9.42	−4.34	0.0563
5/29	9:38	1.1	1200	−9.49	−4.88	−0.0540
	12:33	2.0	1102	−9.58	−5.3	0.0065
	14:54	4.2	1101	−9.51	−5.31	0.0090
	16:10	8.7	1003	−9.21	−5.85	
5/30	15:18	8.4	900	−4.45	−6.3	
6/01	8:55	29.8	900	−4.45	−6.3	
DK7(010)-3, GF = 55.53 m^{-1}, l_i = 0.109 cm, l_i = 0.109 cm						
7/02	15:45	75.1	1200	−7.70	−5.24	
7/06	15:40	18.0	1200	−9.08	−5.15	−0.0493
7/07	16:15	19.0	1200	−11.74	−4.78	−0.0577
7/08	13:13	4.3	1200	−9.07	−5.14	−0.0379
	16:00	13.0	1000	−9.03	−5.99	
7/09	12:00	3.5	1000	−10.00	−5.94	
7/10	9:20	20.6	1000	−13.46	−5.63	−0.0634
	12:45	2.6	1200	−10.82	−4.88	−0.0268
	16:30	10.8	1200	−9.97	−5.02	−0.0459
7/11	11:20	16.3	1000	−12.26	−5.75	−0.0127
7/12	16:00	8.5	1000	−11.34	−5.84	0.0282
7/13	15:10	7.5	1200	−12.32	−4.72	−0.0802
	16:17	8.6	1200	−12.88	−4.70	
7/14	15:40	7.4	1200	−13.33	−4.67	
	16:31	9.6	1200	−13.98	−4.67	
7/16	9:24	24.9	1000	−13.95	−5.51	
	14:40	30.1	1000	−13.95	−5.52	−0.0231

TABLE 3.—*Continued*

Date	Time	Duration (h)	T (°C)	log f_{O_2}	log σ	Residual*
7/17	14:58	21	1000	−13.46	−5.58	−0.0234
7/18	14:40	16.4	1197	−15.01	−4.67	
7/20	11:42	24.2	1000	−14.95	−5.40	−0.0454
7/21	8:18	19.3	1200	−15.05	−4.71	
	16:15	7.2	1002	−15.72	−5.33	
7/22	7:57	22.9	1002	−15.75	−5.35	
7/23	8:15	23.6	1000	−17.29	−5.33	
	18:32	9.6	1200	−8.48	−5.15	
7/24	6:45	21.8	1200	−8.48	−5.17	0.0161
	12:35	3.2	1200	−8.50	−5.18	
7/27	8:54	68.0	1200	−12.01	−4.65	0.0339
	15:21	24.0	1175	−12.00	−4.75	0.0550
7/28	14:10	2.5	1150	−12.01	−4.86	0.0674
	14:40	9.6	1126	−12.00	−5.03	0.0219
7/29	14:00	5.5	1150	−12.00	−4.88	0.0489
	15:36	8.7	1100	−12.0	−5.16	0.0301
7/30	11:45	3.6	1075	−12.01	−5.29	0.0366
	15:33	2.9	1050	−11.99	−5.43	0.0426
7/31	7:10	15.4	1025	−11.98	−5.61	0.0126
	12:28	4.0	1000	−12.00	−5.75	0.0243
	16:02	19.1	975	−11.96	−5.87	
8/01	15:24	9.1	950	−11.96	−6.01	
8/02	6:50	16.5	950	−12.06	−5.96	
8/03	14:00	5.3	925	−12.00	−6.11	
	16:09	15.3	900	−12.00	−6.21	
8/04	13:03	5.0	875	−11.99	−6.30	
	16:00	16.0	850	−12.03	−6.44	
8/05	11:00	2.0	900	−11.99	−6.22	
	14:37	3.3	1000	−12.00	−5.78	−0.0057
	18:51	3.9	1100	−12.01	−5.20	−0.0113
8/06	7:45	12.5	1200	−12.00	−4.63	0.0553
	DK7(001)-2; GF = 8.70 m^{-1}, l_i = 0.96 cm, l_t = 0.095 cm					
3/11	15:50	59.0	1200	−8.43	−4.658	0.0529
3/12	14:55	5.2	1300	−7.31	−4.30	0.0959
3/13	12:45	0.7	1200	−8.42	−4.753	−0.0413
	14:45	0.8	1101	−9.76	−5.14	−0.0801
	15:25	7.0	1100	−9.77	−5.14	−0.0763
3/14	10:43	6.0	1000	−11.25	−5.54	−0.0581
3/15	13:03	6.0	900	−12.90	−5.96	0.0236
3/16	12:45	4.2	800	−15.05	−6.51	0.0407
	16:15	16.0	800	−15.00	−6.50	0.0580
3/17	11:00	2.4	1200	−8.45	−4.72	−0.0120
	13:00	1.0	1300	−7.32	−4.34	0.0544
	16:20	9.2	1250	−7.87	−4.53	0.0156
3/18	8:46	0.6	1150	−9.10	−4.93	−0.0524
3/19	15:10	27.0	1200	−11.89	−4.16	0.0473
3/20	15:15	3.0	1200	−12.43	−4.12	0.0087
	22:16	10.0	1200	−12.44	−4.11	0.0142
3/21	16:45	6.4	1200	−10.15	−4.45	0.0106
3/23	13:55	19.6	1200	−8.02	−4.86	−0.0898
3/24	8:15	17.6	1200	−3.33	−5.20	
	11:30	2.0	1200	−5.47	−5.08	0.0618
	12:25	2.8	1200	−5.57	−5.08	0.0472
	13:55	0.8	1000	−8.79	−5.90	−0.0600
	15:45	1.3	1001	−7.59	−6.00	0.0079
3/24	16:12	10.1	1002	−7.55	−6.03	−0.0231
3/25	9:15	0.4	1000	−3.13	−6.19	
	9:55	1.1	1000	−3.26	−6.13	
	13:12	3.0	1200	−12.45	−4.18	−0.0542
	14:19	0.9	1000	−15.67	−4.83	0.0086
	17:00	2.0	1200	−14.37	−4.15	
	17:17	8.0	1199	−14.39	−4.10	
3/26	9:00	1.2	1001	−17.47	−4.75	
	Mal(100)-1, GF = 35.38 m^{-1}, l_i = 0.142 cm, l_t = 0.142 cm					
8/07	10:23	18.4	1200	−9.93	−3.74	
	16:09	32.1	1200	−9.93	−3.73	
8/10	9:05	89.1	1200	−9.93	−3.76	
	13:05	93.1	1200	−9.93	−3.76	−0.0408
	16:35	10.8	1200	−8.15	−3.78	−0.0029
8/11	16:38	8.5	1200	−13.61	−3.63	

TABLE 3.—*Continued*

Date	Time	Duration (h)	T (°C)	log f_{O_2}	log σ	Residual*
8/12	8:32	16.5	1200	−13.63	−3.63	−0.0313
	11:37	1.6	1000	−17.01	−4.65	
	14:55	4.9	1000	−17.07	−4.67	
	16:50	8.6	1000	−15.2	−4.38	
8/13	8:25	16.2	1000	−15.32	−4.44	
	12:23	1.3	1000	−16.19	−4.59	
	16:04	5.0	1000	−16.18	−4.75	
8/14	8:22	15.5	1000	−11.38	−4.45	
	11:08	1.0	1100	−11.38	−3.96	
	15:12	5.1	1101	−11.36	−3.95	−0.0503
	16:50	8.7	1200	−11.28	−3.70	
8/17	8:26	64.7	1200	−11.27	−3.67	0.0055
	10:44	1.2	1200	−12.20	−3.60	
	14:24	4.9	1200	−12.20	−3.63	0.0152
8/18	9:00	17.4	1200	−13.02	−3.59	0.0282
	11:30	1.6	1175	−13.02	−3.69	−0.0170
	15:09	1.0	1150	−13.02	−3.74	−0.0107
	16:05	8.2	1125	−13.02	−3.76	
8/19	8:15	16.3	1125	−13.02	−3.79	−0.0203
	9:52	1.0	1100	−13.02	−3.83	0.0181
	14:02	2.0	1075	−13.02	−3.92	−0.0095
	15:45	8.75	1051	−13.02	−4.02	−0.0467
8/20	10:00	1.7	1025	−13.03	−4.17	
	13:00	2.7	1000	−13.03	−4.30	
	15:10	1.2	975	−13.00	−4.48	
	16:16	2.3	975	−13.02	−4.49	
8/21	9:55	2.1	950	−13.03	−4.65	
	13:26	3.7	925	−13.03	−4.84	
	15:50	8.4	900	−13.02	−5.14	
8/24	12:15	3.2	850	−13.02	−5.52	
8/26	12:21	46.6	800	−13.03	−6.1	
	16:00	5.5	900	−13.01	−5.12	
8/27	13:52	5.0	1000	−13.03	−4.33	
8/28	7:30	16.7	1100	−13.02	−3.83	0.0181
	9:57	1.0	1200	−13.00	−3.60	0.0192
	11:00	24.4	1200	−9.03	−3.74	
8/31	9:45	71.3	1200	−9.03	−3.75	
	14:15	75.3	1200	−9.03	−3.75	−0.0015
	17:06	12.0	1102	−8.96	−3.97	
9/01	8:27	17.3	1100	−8.98	−3.97	0.0097
	16:39	16.6	1000	−8.97	−4.48	
9/02	15:35	16.0	900	−9.10	−5.15	
9/03	10:29	24.9	900	−9.02	−5.10	
	16:22	18.4	850	−9.05	−4.73	
9/04	9:38	20.0	850	−9.2	−5.01	
	11:08	21.5	850	−9.4	−5.15	
	14:27	24.0	850	−9.6	−5.19	
	15:46	0.3	1100	−8.97	−3.97	
	16:13	0.8	1100	−8.96	−3.97	
9/05	15:55	24.5	1100	−9.00	−3.98	−0.0009
9/08	12:00	0.2	1100	−12.94	−3.80	
	12:15	0.5	1100	−12.95	−3.795	
	13:00	1.2	1100	−12.95	−3.80	
	13:45	2.0	1100	−12.95	−3.79	
9/09	7:45	20.0	1100	−12.97	−3.79	0.0598
9/10	9:00	23.5	1100	−9.28	−3.93	0.0400
	2.42-MΩ resistor, expected log σ = −6.380 to −6.388					
9/15	14:40				−6.39	
	36.3-MΩ resistor, expected log σ = −7.556 to −7.564					
	15:45				−7.54	
	Mal(010)-1, GF = 8.68 m^{-1}, l_i = 0.144 cm, l_t = 0.145 cm					
4/29			1225	−9.54	−3.59	0.0051
			1125	−10.87	−3.80	0.0223
			1025	−12.37	−4.06	0.0252
5/01			1225	−7.58	−3.67	−0.0388
			1125	−8.87	−3.82	0.0391
			1025	−10.37	−4.11	0.0120
5/02			1225	−11.57	−3.56	−0.0023
			1125	−12.88	−3.74	0.0453
			1025	−14.41	−4.01	0.0376

continued

TABLE 3.—*Continued*

Date	Time	Duration (h)	T (°C)	$\log f_{O_2}$	$\log \sigma$	Residual*
5/08			1223	−11.59	−3.56	0.0020
5/12			1125	−12.86	−3.82	−0.0343
5/13			1025	−14.40	−4.11	−0.0622
			975	−15.22	−4.22	−0.0246
5/14			1225	−9.54	−3.61	−0.0149
5/15			1225	−9.54	−3.64	−0.0449
5/20			1225	−12.57	−3.53	0.0093
			1225	−12.57	−3.53	0.0093
			1125	−13.87	−3.72	0.0471
			1025	−15.39	−4.03	−0.0005
			975	−16.22	−4.22	−0.0430
			900	−17.61	−4.41	0.0114

Note: Where a resistor is designated, a precision resistor was substituted for the sample and electrodes. Where a pyroxene plate is designated, GF is its geometric factor, l_i and l_f are its initial and final thicknesses (see text).

* Residual is the observed log σ minus the calculated log σ; for calculated log σ, see least-squares fitting parameters in Table 5.

therms in $\log f_{O_2}$–$\log \sigma$ space. Conductivity measurements in the central part of the investigated f_{O_2} range appear to have a linear dependence on f_{O_2} and were fit to the expression

$$\log \sigma = A_0 + B/T + N(\log f_{O_2})$$

by using ORGLS2, the general nonlinear least-squares program of Busing and Levy (1962), where T is temperature in kelvins. Each data set was fit to 0.03–0.07 σ unit (one standard error of an observation). Because the possible systematic errors in the measurement technique are of the same magnitude, we did not try to improve the fit by using higher-order terms to, for instance, identify a possible temperature dependence of B, which is proportional to the thermal activation energy.

RESULTS

Impedance spectra at a variety of temperatures and oxygen-fugacity values were obtained perpendicular to (100), (010), and (001) plates of crystal DK7 and (100) and (010) plates of MAL, all at 1-bar pressure. Typical spectra are shown in Figure 3. For DK7, impedance is usually independent of frequency below about 500 Hz, and the phase angle θ is close to 0° (dispersion is small). However, for the more-Fe-rich MAL diopside and, to a slight extent, some spectra of the (010) orientation of DK7 at low f_{O_2} values, there appear to be high-frequency–low-impedance and low-frequency–high-impedance regimes distinguished by the decrease of impedance with frequency and separated by frequency intervals in which θ is negative. The use of metallic electrodes was intended to block the passage of all pyroxene components except electrons. In practice the electrodes conducted electrons, allowed oxygen to pass, probably by leakage along the electrode-sample interface, and provided no mechanism for supplying or removing the cationic species in diopside. The fact that most diopside spectra show no increase of impedance at very low frequency suggests that ions are not accumulating at the crystal-electrode interfaces, even at 0.0001 Hz. Thus polarization does not appear to be significant for most DK7 plates but does appear to be significant for MAL diopside at low frequencies. The exact cause is not yet understood, but possibilities will be discussed in a subsequent paper that deals with the signatures of the components that contribute to an imped-

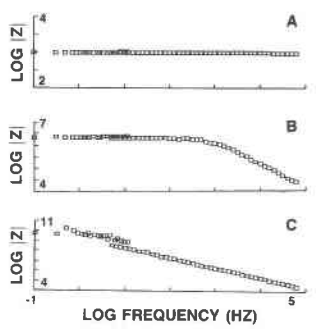

Fig. 2. Impedance spectra used to verify conductivity measurements and demonstrate insignificant leakage paths at room temperature. In each case a Teflon plate, 0.86 mm thick and 16 mm in diameter, was positioned between the electrodes in the position normally occupied by diopside plates and a representative value of the geometric factor is incorporated in the data. (**A**) 10-kΩ resistor in parallel with electrodes. (**B**) 20-MΩ resistor in parallel with electrodes. (**C**) No resistor (∞ Ω) in parallel with electrodes.

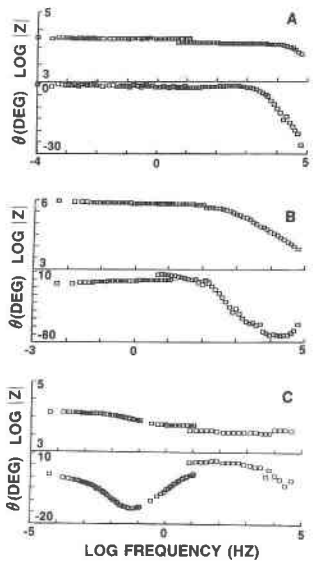

Fig. 3. Representative impedance spectra of diopside, showing plots of impedance (Z) and phase angle (θ). The transition from low-frequency FFT to high-frequency lock-in measurements at 10 Hz causes a slight discontinuity. The decrease in Z at high frequency is due to the capacitance effects of the electrodes, leads, and measurement circuit. (**A** and **B**) For DK7, the impedance is flat over most of the frequency range and specifically does not increase with decreasing frequency. (**C**) The impedance of the Fe-bearing diopside from Malacacheta increases with decreasing frequency. This effect, which we have also observed in olivine, might be caused by polarization at the blocking electrodes. (**A**) Plate DK7(001)-2, 1200 °C, $\log f_{O_2} = -14.39$. (**B**) Plate DK7(100)-2, 1000 °C, $\log f_{O_2} = -7.58$. (**C**) Plate MAL(010)-1, 1225 °C, $\log f_{O_2} = -9.60$.

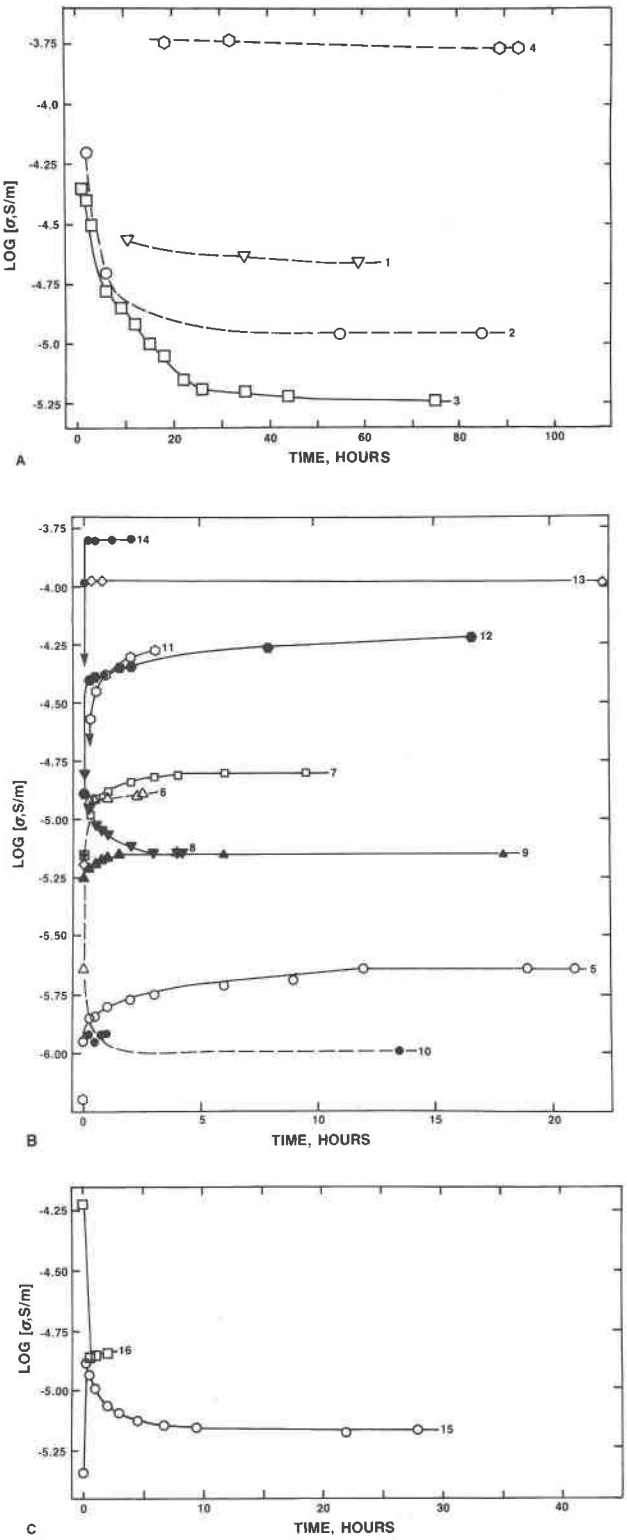

Fig. 4. Response, as a function of time, of conductivity to changes in temperature and oxygen fugacity. (**A**) On the initial heating, the conductivity of DK7 plates decreases relatively slowly as if they previously had been more reducing. (**B**) When furnace conditions change, re-equilibration is reversible and relatively rapid. The response to temperature changes used in this work is faster than the response to changes in oxygen fugacity. (**C**) The responses of conductivity to temperature and f_{O_2} are opposite in sense, and the response to temperature change is faster than the response to change in f_{O_2}. Thus, when the temperature and f_{O_2} both decrease (or both increase), the conductivity of DK7 diopside passes through a maximum (minimum). The sample numbers and conditions represented by each curve are shown in Table 4.

Table 4. Sample numbers and conditions for curves in Figure 4

Curve	Sample	T_i (°C)	$\log(f_{O_2})_i$	T_f (°C)	$\log(f_{O_2})_f$
1	DK7(001)-2	25	−0.7	1200	−8.4
2	DK7(010)-2	25	−0.7	1200	−8.5
3	DK7(010)-3	25	−0.7	1200	−7.7
4	MAL(100)-1	25	−0.7	1200	−9.9
5	DK7(010)-3	1000	−10.0	1000	−13.5
6	DK7(010)-3	1000	−13.5	1200	−10.8
7	DK7(010)-3	1200	−9.1	1200	−11.7
8	DK7(010)-3	1200	−11.2	1200	−9.1
9	DK7(010)-3	1200	−7.7	1000	−9.1
10	DK7(010)-3	1200	−9.1	1000	−9.1
11	DK7(001)-2	1000	−3.2	1200	−12.4
12	DK7(001)-2	1000	−15.7	1200	−14.4
13	MAL(100)-1	850	−9.6	1100	−9.0
14	MAL(100)-1	1100	−9.0	1100	−13.0
15	DK7(010)-3	1100	−17.3	1200	−8.5
16	DK7(001)-2	1200	−14.4	1000	−17.5

ance spectrum. For most spectra, the phase angle was approximately 0° in the frequency range 0.01 to 1 kHz. Above 1 kHz, the impedance falls in all the spectra, including those of Teflon, alumina, silica glass, and networks of standard components. Simple calculations based on the geometry of the electrode assembly and leads predict a similar response. Thus, we attribute this high-frequency behavior as due simply to the capacitance of the metal electrodes, leads, and the measuring circuit (compare Figs. 2 and 3). Some other measuring techniques compensate for these components during the measuring process so that these effects are not readily seen. It is clear that had we relied on measurements made at a single frequency in the commonly used frequency range 1.0–1.7 kHz, the conductivity would have been sensitive to frequency and perhaps reflect components of conductivity that are not associated with the interior of the sample. The polarization of MAL diopside did interfere with the impedance determination, but only at 800 °C. At this low temperature, the changes in impedance (decrease with increasing frequency) due to polarization and to the capacitance of the electrodes and leads were indistinguishable. The maximum value of the phase θ was only $-10°$ (at 13 Hz), causing a small error in the reported impedance for that measurement. Critical conductivity values for each spectrum are tabulated in Table 3.

The immediately preceding temperature-f_{O_2}-time history of a sample affects the manner in which a sample responds to changes in the furnace environment. When

TABLE 5. Fit parameters of conductivity, diopside

	log A_0	A_0	Q (eV)	N	No. of measurements	T (°C)
DK7(100)-2	1.434 ± 0.202	27.16	2.154 ± 0.016	−0.1776 ± 0.0065	26	1000–1300
DK7(010)-1,2	1.075 ± 0.148	11.89	2.009 ± 0.045	−0.1023 ± 0.0093	25	900–1300
DK7(010)-3	0.540 ± 0.163	3.46	2.026 ± 0.048	−0.1423 ± 0.0078	26	≥1000
DK7(010) avg.	0.885	7.68	2.018	−0.1223		
DK7(001)-2	1.583 ± 0.101	38.28	2.198 ± 0.033	−0.1456 ± 0.0048	25	800–1300
DK7 avg.	1.39	24.4	2.12	−0.15		
MAL(100)-1	−0.890 ± 0.184	0.129	0.922 ± 0.052	−0.0326 ± 0.0037	17	1050–1200
MAL(010)-1	−0.252 ± 0.111	0.56	1.046 ± 0.040	−0.0184 ± 0.0044	21	900–1225
MAL avg.	−0.46	0.34	0.98	−0.026		

Note: $\log \sigma = \log A_0 + [-Q/RT] + N(\log f_{O_2})$, where σ is conductivity in siemens per meter, Q is in electronvolts, T is in kelvins, N is a constant, and f_{O_2} is in bars.

first placed in the furnace, plates were allowed to equilibrate with the furnace atmosphere at 1200 °C for several days. The conductivity of DK7 diopside decreased monotonically with time, falling as much as one log σ unit and requiring as much as 45 h to stabilize (Fig. 4A, Table 4). In contrast, when first heated, MAL diopside equilibrated rapidly. For subsequent changes in temperature at constant f_{O_2}, steady-state values of conductivity were usually achieved within 5 h (Fig. 4B). Equilibration of DK7 diopside was slowest in a very reducing environment. MAL diopside equilibrated within minutes. In several cases involving DK7 diopside, the conductivity passed through a maximum or minimum (Fig. 4C), suggestive of competing processes with different rate constants. With the exception of the first heating (for which the initial state of the sample is unknown), measured conductivities were reversible with respect to changes in both temperature and f_{O_2}, a fact that can readily be gleaned from Table 3 because the measurements for each sample are reported in the sequence in which they were obtained. To reduce the time needed for equilibration, we adopted a strategy of following oxygen isobars, rather than isotherms, whenever possible, and of changing f_{O_2} at high temperature (1200–1300 °C) to hasten equilibration with the furnace atmosphere.

Our initial approach was to explore log σ–log f_{O_2} space for DK7 diopside at various temperatures. Isotherms are plotted in Figure 5. At constant temperature, conductivity decreases with increasing f_{O_2} throughout much of the range that is easily obtained with CO + CO_2 furnace-gas mixtures. The log f_{O_2}–temperature relationships of the oxygen-buffer assemblages iron + wüstite + vapor (IW) and quartz + fayalite + magnetite + vapor (QFM) are indicated because these reactions define a volume (in T, P, f_{O_2} space) that encompasses many igneous and metamorphic processes in the crust. (The buffer reactions are shown for convenience only. They are *not* meant to imply that equilibrium among Fe species controls the conductivity!) Conductivity *decreases* with increasing f_{O_2} [$\partial(\log \sigma)/\partial(\log f_{O_2}) \approx -1/7$] throughout this f_{O_2} range. Least-squares fitting parameters for data in this range are given in Table 5, and residuals (observed minus calculated value of log σ) are included in Table 3.

The MAL diopside behaves differently (Fig. 6) but not entirely as anticipated. We expected that its conductivity would be greater than in DK7 because Cr^{3+}, which is present in MAL diopside, has been associated with increased conductivity in orthopyroxene [compare the results for crystals #173 (Duba et al., 1973) and MF#1–3 (Huebner et al., 1979)] and because an increase in Fe/(Mg + Fe) is associated with increased conductivity in synthetic olivine (Hinze et al., 1981) and orthopyroxene (Voigt et al., 1979) aggregates. This expectation was realized. We also expected that the significant Fe content of the MAL diopside might have caused the conductivity to increase with oxygen fugacity as it does with olivine (Cemic et al., 1980; Schock and Duba, 1985), but we observed a slight *decrease.* Within measurement uncertainties, this observation is consistent with the observations of Huebner et al. (1979, their Fig. 2) who found no dependence of log σ on log f_{O_2} in impure Fe-bearing orthopyroxenes. At ≤900 °C, the behavior pattern of MAL changes, suggesting a positive slope of $\partial(\log \sigma)/\partial(\log f_{O_2})$. At 1000 °C and log $f_{O_2} < -15$, the measurements were unstable. Schock and Duba (1985) associated unstable readings with reduction and loss of Fe from olivine. Because we could subsequently reproduce earlier measurements at 1100–1200 °C and found no evidence of reduction when the sample was removed from the furnace, we do not think that our experiments were troubled by reduction of Fe.

Oxygen isobars in conductivity–temperature space (Fig. 7) were carefully determined for one orientation each of DK7 (at log $f_{O_2} = -12.0$) and MAL (log $f_{O_2} = -13.0$). The data are reversible with respect to temperature, each isobar can be described by two straight line segments, and the transition between segments occurs over a narrow temperature range. The slope [$\partial(\log \sigma)/\partial(1/T)$, where T is in kelvins] decreases with decreasing temperature for DK7 but increases with decreasing temperature in the case of MAL diopside. DK7 behaves like other pyroxenes (Duba et al., 1973; Huebner et al., 1979; Duba et al., 1979) and

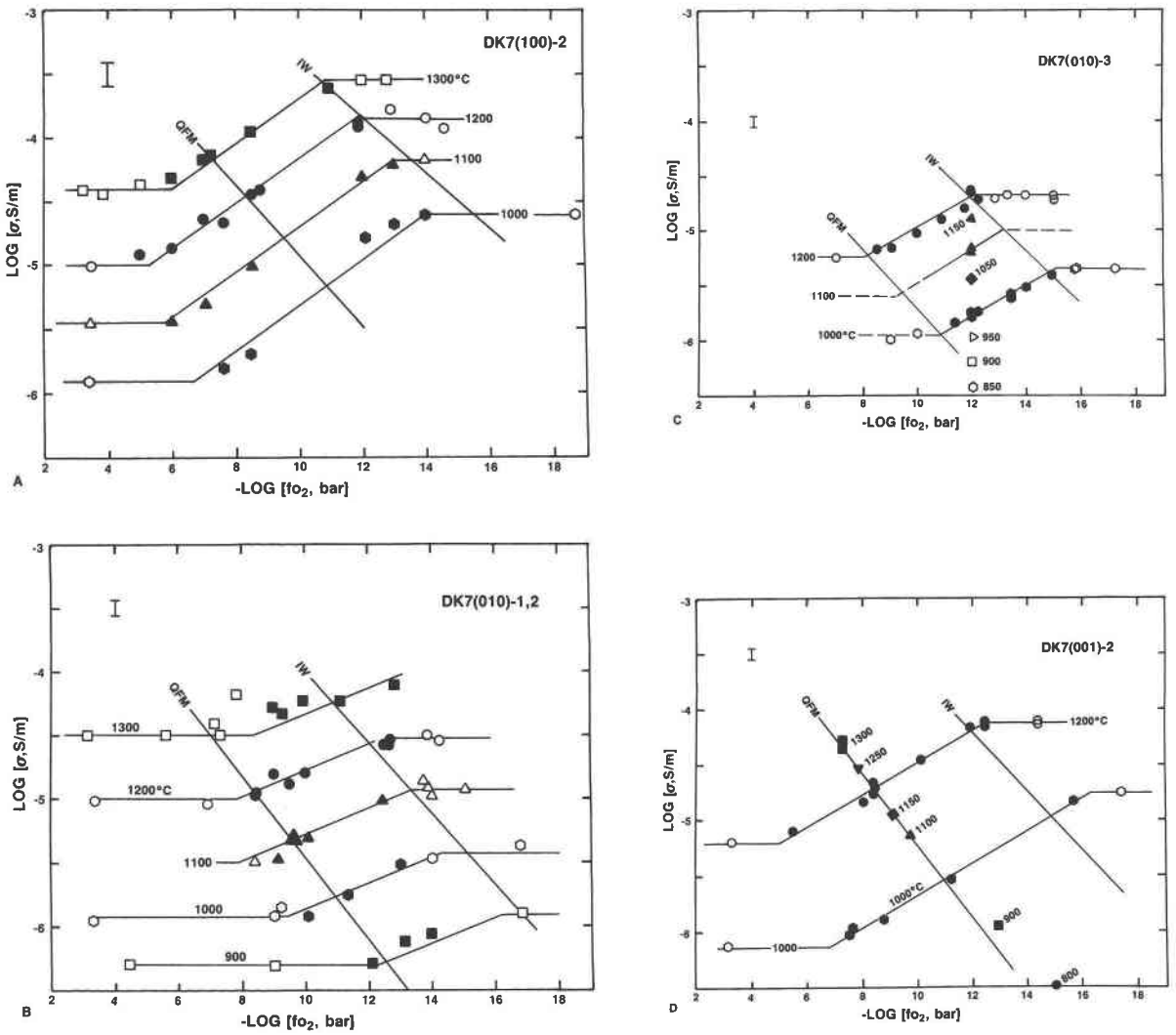

Fig. 5. Electrical conductivity values for three orientations of diopside DK7 (nearly end-member $CaMgSi_2O_6$). Conductivities are measured perpendicular to each plate and projected from temperature onto the log σ–log f_{O_2} plane at 1-bar pressure. Solid symbols represent some of the data (Table 3) used in the regressions (Table 5); regressed data are those with an entry in the right-hand column of Table 3. Vertical bar represents one standard error in log σ for each data set. Projections of the oxygen-buffer assemblages iron-wüstite-vapor (IW) and fayalite-magnetite-quartz-vapor (FMQ) indicate the range within which most igneous and metamorphic rocks will fall, but are not meant to imply that equilibrium among Fe species controls the conductivity. Results for first and second (010) plates (**B**) are similar, but the third (010) plate (**C**) appears to be less conductive. This difference may be due to differences in the nature of the sample-electrode contact.

olivines (Duba and Nichols, 1973; Cemic et al., 1980) in that the slope invariably decreases at lower temperature, if it changes at all. The behavior of the MAL diopside is without precedent, yet these data at log $f_{O_2} = -13.0$ are reversible and otherwise internally consistent. The facts that the slope steepens and that the measured impedances (before application of the geometric factor) of MAL(100)-1 are less than those of the single-crystal alumina both suggest that an unanticipated electrical path around the sample (leakage) is not an explanation for the strange behavior of MAL. Further, the fact that the change in slope occurs at an f_{O_2} value that is above that of the iron-wüstite assemblage (the IW buffer intersects the log $f_{O_2} = -13$ isobar at ~1120 °C) suggests that reduction of the sample is not an explanation.

The observed variation in density with f_{O_2} is pronounced and systematic (Table 2). The density of oxidized DK7 is 0.017 g/cm³ (0.5%) greater than reduced DK7. Similarly, oxidized MAL is 0.027 g/cm³ (0.8%) greater than reduced MAL. The cell volumes, determined on splits of the chips used for the density measurements, change by only marginally significant amounts, +0.1% and −0.2%, respectively. Thus, the unit-cell contents of DK7 and MAL diopside must increase in mass as furnace f_{O_2} is increased. Finally, the thicknesses of the pyroxene plates did not change as a result of the temperature pro-

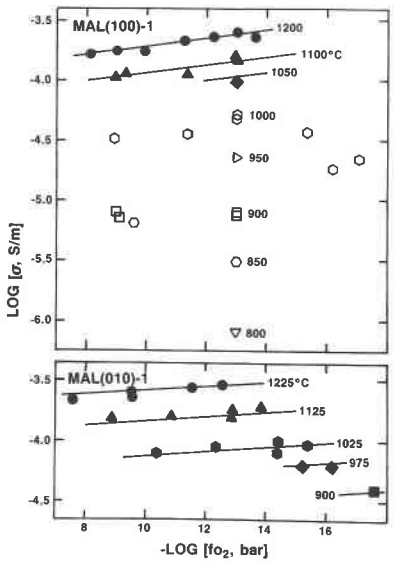

Fig. 6. Isotherms of electrical conductivity measured perpendicular to (100) and (010) plates of MAL diopside and plotted as a function of oxygen fugacity. As in Fig. 5, solid symbols represent data used to obtain the regressions and the positions of the iron-wüstite (IW) and quartz-fayalite-magnetite (QFM) assemblages are shown for convenience. At 1000–1225 °C, the conductivity of MAL diopside is greater than that of DK7 diopside and is almost independent of f_{O_2}, but at the lower temperatures, the behavior changes, suggesting a change in conduction mechanism.

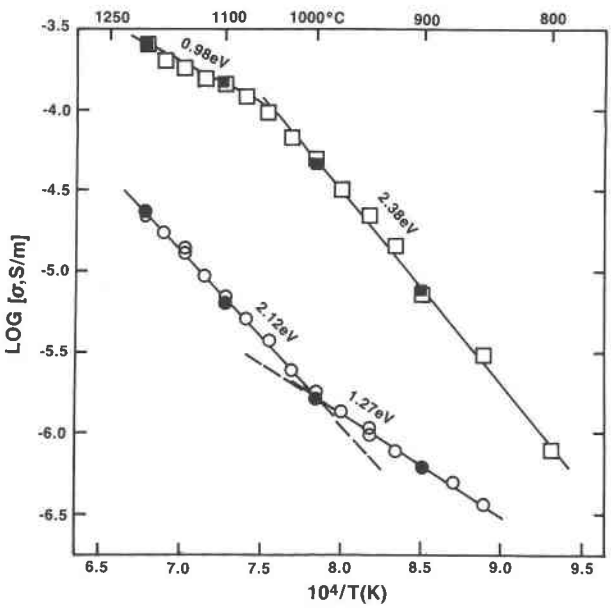

Fig. 7. Oxygen isobars of conductivity versus temperature. Squares are measured values for MAL(100)-1 at $\log f_{O_2} = -13.0$ (f_{O_2} in bars); circles are values for DK7(010)-3 at $\log f_{O_2} = -12.0$. Open symbols signify that temperature was decreased before the measurement was taken; closed symbols indicate that temperature was increased. The straight-line relationship was drawn to pass through the measurements that were bracketed with respect to direction of temperature change. Activation energies (Q, see text) are shown. The break in slope for DK7(010) can be explained by the presence of two mechanisms, the mechanism with $Q = -2.12$ eV being dominant at high temperature and the mechanism with $Q = -1.27$ eV being dominant at low temperature. The break in slope for MAL (100) cannot be explained by the coexistance of only two mechanisms, one of which is dominant at high temperature and the other dominant at low temperature.

cess (Table 3). This admittedly imprecise determination of plate thickness, when combined with the constancy of cell dimensions (Table 2), suggests that the number of unit cells in a diopside plate was not changed drastically by exposure to furnace conditions.

Discussion

The conductivity ranges of hypothetical isotropic (randomly oriented) aggregates of DK7 and MAL diopsides, calculated by averaging our results for the different crystallographic orientations, overlap the range for mantle olivines (composition Fo_{100} to Fo_{91}) but are less conducting than orthopyroxenes and plagioclase (Fig. 8). By analogy with end-member Fo_{100} (Pluschkell and Engell, 1968; Schock and Duba, 1985), which is less conducting than olivines Fo_{96} and Fo_{91} (Duba et al., 1974; Schock and Duba, 1985), it is not surprising that DK7 diopside is more insulating than Fe-rich pyroxenes. But it is surprising that the $-1/7$ dependence of $\log \sigma$ on $\log f_{O_2}$—which is observed in synthetic forsterite, Fo_{100}, but not in either $Fo_{99.8}$ (T. Parkin, 1972, cited in Schock and Duba, 1985) or any previously measured pyroxene—is present in a natural diopside. Apparently the small amounts of Fe [Fe/(Mg + Fe) = 0.027] and perhaps Al and Na in DK7 are not sufficient to modify its behavior from what we presume to be the behavior pattern of pure end-member $CaMgSi_2O_6$. Thus, it would be no more appropriate to use the DK7 diopside to model the electrical conductivity of augite (in planetary mantles) than it would be to use the data for pure forsterite to model mantle olivine. The green MAL diopside is a much more appropriate model for the conductivity of mantle augite. Its use as an analogue is simplified by the absence of a strong $\log f_{O_2}$ dependence.

The principal goal of this investigation is to identify point defects that might enhance electrical conductivity and other transport properties such as chemical diffusion. This process of identification proceeds from relationships between conductivity and composition and from measured activation energies. The work of Stocker (1978a) provides an excellent framework. He tabulated point-defect reactions that might occur in enstatite, $(Mg,Fe)_2SiO_6$, and distinguished reactions that can occur in a closed system, a system open only to O_2, and a system allowed to exchange all of its components with other phases. Our measurement technique is that of a system presumably open only to O_2. The nominal diopside bulk composition differs from that of enstatite in having the M2 site filled largely with Ca, rather than Mg and Fe. Because Ca ions

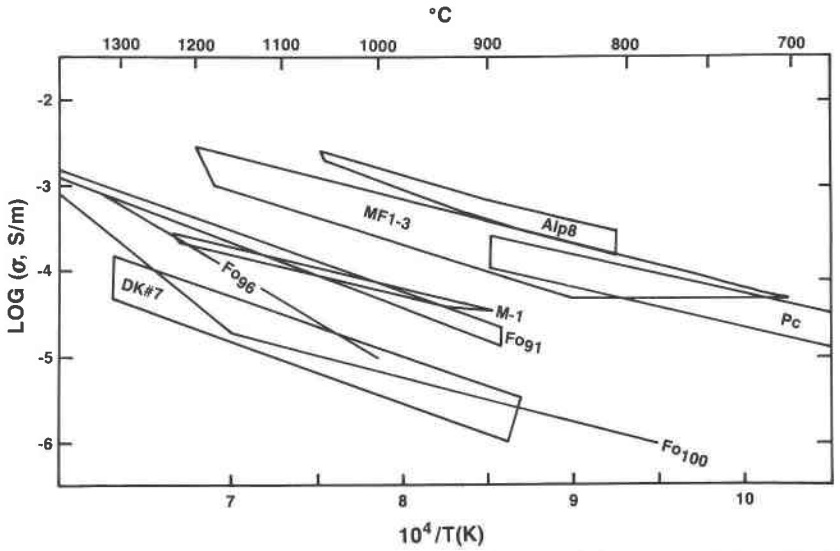

Fig. 8. Ranges of conductivity at 1-bar total pressure of single-crystal analogues of phases related to those that occur in the lower crust and mantle at higher pressures. DK7 and MAL diopside conductivities are shown as enclosed regions bounded by the oxygen isobars QFM (at low conductivity) and IW (high conductivity). Like pure forsterite, Fo_{100}, almost pure diopside DK7 conducts poorly. The Fe-bearing diopside, M-1, has conductivity similar to olivine Fo_{91}, with Fe/(Mg + Fe) = 0.095, distinctly less than impure orthopyroxenes and plagioclase. Sources of data: DK7 and M-1 clinopyroxenes, this study; Alp-8 orthopyroxene, Duba et al. (1979); MF1-3 orthopyroxenes, Huebner et al. (1979); Pc plagioclase, Maury (1968); Fo_{91}, Fo_{96}, and Fo_{100} olivines and forsterite, Duba et al. (1974). M-1 is MAL elsewhere in text.

are large and cannot easily be oxidized, they are highly unlikely to form paired vacancies and interstitials (the Ca Frenkel reaction). Because our measurement system is closed to all components but O_2, Ca cannot exchange with external phases. We conclude that Ca will be less a defect-former than the Mg and Fe it replaces in the enstatite model. Thus the enstatite defect structure is a suitable model for that of diopside, and Stocker's analysis provides a suitable framework for interpreting our measurements of initially stoichiometric or nearly stoichiometric crystals.

The electrical conductivity of a species i is proportional to its concentration c and its mechanical mobility B_i (see Rickert, 1982, p. 84–86):

$$\sigma_i = c_i B_i z^2 eF$$

where z, e, and F are valence, charge, and Faraday constant. (Mechanical mobility is related to electrical mobility μ through the expression $\mu_i = zeB_i$.) To understand the conduction mechanism in diopside DK7, we must identify a reaction in which the concentration (c_i) of a charge-carrying species varies according to $c_i \propto (f_{O_2})^N$, where $N = -1/(7 \pm 1)$ (see Table 5) and all other aspects of the bulk composition remain constant. We consider four reactions. Using the defect-species notation of Kröger (1974, p. 14), Reaction 1 involves the incorporation of oxygen to form oxygen interstitials (I) and to leave electron holes (h) in the valence band:

$$O_2 = 2O_I'' + 4h^\cdot \qquad (1)$$

$$K_1(f_{O_2}) = [O_I'']^2[h^\cdot]^4.$$

Since each oxygen interstitial causes the formation of two holes,

$$[h^\cdot] = 2[O_I'']$$

$$K_1''(f_{O_2}) = [h^\cdot]^2[h^\cdot]^4$$

and

$$[h^\cdot] \propto (f_{O_2})^{1/6}.$$

According to this reaction, the defect concentration increases with oxygen fugacity, an effect that is opposite to the relationship that we observed. In addition, some workers regard oxygen interstitials as being too large to be accommodated in the pyroxene structure (see Stocker, 1978a). In olivine, oxygen interstitials and electron holes probably are energetically unfavorable defects (Stocker, 1978b).

Reaction 2 results in the formation of Si vacancies:

$$3O_2 = 2V_{Mg}'' + 2V_{Si}'''' + 6O_O^\times + 12h^\cdot \qquad (2)$$

$$K_2(f_{O_2})^3 = [V_{Mg}'']^2[V_{Si}'''']^2[O_O^\times]^6[h^\cdot]^{12}.$$

Since the concentration of oxygen on oxygen lattice sites is close to the standard-state concentration, $[O_O^\times]^6 \approx 1$. Further, each Mg and Si vacancy create two and four holes, respectively, leading to the expression

$$K_2'(f_{O_2})^3 = [h^\cdot]^2[h^\cdot]^2[h^\cdot]^{12}$$

and

$$[h^\cdot] \approx (f_{O_2})^{3/16}.$$

This expression also predicts an f_{O_2} dependence of the conductivity that is opposite to that observed. We consider Si vacancies [V_{Si}''''] to be energetically unfavorable in the pyroxene structure, which is based on tightly bound SiO_4 units. Stocker and Smyth (1978) reached a similar conclusion when considering possible defects in olivine.

Reaction 3 involves cation interstitials:

$$2Mg_{Mg}^{\times} + 2Si_{Si}^{\times} + 6O_O^{\times} = 3O_2 + 2Mg_i^{\cdot\cdot} + 2Si_i^{\cdot\cdot\cdot\cdot} + 12e' \quad (3)$$

$$K_3 = (f_{O_2})^3[Mg_i^{\cdot\cdot}]^2[Si_i^{\cdot\cdot\cdot\cdot}]^2[e']^{12}.$$

Since Mg and Si interstitials create 2 and 4 electrons, respectively,

$$K_3' = (f_{O_2})^3[e']^2[e']^2[e']^{12}$$

and

$$c_i \propto [e'] = K_3'(f_{O_2})^{-3/16}.$$

This oxygen-fugacity dependence is slightly larger than that measured for DK7(100)-2 and significantly larger than found for all other DK plates (Table 5). Continuing the analogy with olivine (Stocker and Smyth, 1978), Mg and Si interstitials have lower defect energies, and are thus more likely to form, than the oxygen interstitials and Si vacancies of the first two reactions.

Reaction 4 involves oxygen vacancies, which are estimated to have intermediate formation energies in olivine (Stocker, 1978b):

$$4O_O^{\times} = 2O_2 + 4V_O^{\cdot\cdot} + 8e' \quad (4)$$

$$K_4 = (f_{O_2})^2[V_O^{\cdot\cdot}]^4[e']^8/[O_O^{\times}]^4.$$

As before, if the oxygen-vacancy concentration is small, the activity of oxygen ions on normally occupied oxygen lattice sites is close to unity, and

$$K_4(f_{O_2})^{-1/2} = [V_O^{\cdot\cdot}][e']^2.$$

To preserve charge neutrality, each vacancy creates two electrons:

$$[e'] = 2[V_O^{\cdot\cdot}]$$

so that

$$K_4(f_{O_2})^{-1/2} = ([e'][e']^2)/2$$

$$[e'] = K_4'(f_{O_2})^{-1/6}$$

and

$$\sigma = [K_4'(f_{O_2})^{-1/6}]B_i z^2 eF.$$

This f_{O_2} dependence is close to the observed dependence for DK7 diopside. Thus, the observed changes in conductivity with f_{O_2} are better accounted for by the simple formation or destruction of oxygen vacancies (Reaction 4) than by the elimination of diopside unit cells, leaving cation interstitials in the residual diopside and forming oxygen vapor (Reaction 3). The fact that the log σ–log f_{O_2} relation is linear over an interval of several log f_{O_2} units suggests that a single reaction, or a combination of reactions whose proportionate contribution to conduction is constant over the range of interest, is operative. (Had the observed f_{O_2} dependence been caused by a combination of two or more f_{O_2}-dependent mechanisms with different ranges, one would have expected a break in slope with a narrow transition range between two different f_{O_2}-dependent regimes, a highly coincidental situation not revealed by the data.)

Additional considerations led us to favor Reaction 4, by which oxygen vacancies are formed, as the mechanism that is responsible for the observed dependence of log σ on log f_{O_2}. Most important is the observation that the mass of a diopside unit cell increases with increasing f_{O_2} (and vice versa), whereas the number of diopside unit cells remains constant. The change in mass indicates that oxygen moves into (or out of) diopside in response to changes in f_{O_2}, in accord with either Reactions 3 or 4. But Reaction 3 requires that four interstitial cations be formed for each six oxygen atoms that leave the diopside plate, corresponding to the destruction of a unit cell. Thus, the constancy of the number of unit cells is incompatible with Reaction 3. Less compelling considerations are that Reaction 4 is likely to operate in olivine (see discussion by Smyth and Stocker, 1978, p. 188) and is simpler than Reaction 3.

The fact that a defect-forming reaction can explain the observed log σ—log f_{O_2} relationship does not prove that the corresponding defects are the dominant defects in diopside DK7, but the fact that the conductivity increases by almost an order of magnitude with change in f_{O_2} does indicate that the defect reaction is principally responsible for the observed conductivity, at least at low f_{O_2}. The charge carriers are not positively identified by these reactions, but if the mobilities are independent of f_{O_2}, the charge carrier concentration must vary inversely with log f_{O_2}. The possible carriers are electrons, cation interstitials, or oxygen vacancies. An argument in favor of small mobile charge carriers (electrons) is the observation that the conductivity is relatively isotropic. An argument against cations is the observation that conductivity does not decrease with frequency, as would be expected if cations accumulated at the interface with the blocking electrodes.

The relatively high conductivity of MAL diopside, the lack of a strong dependence of conductivity on f_{O_2}, and the smaller activation energy clearly indicate that the conductivity is controlled by a mechanism that is different from the mechanism responsible for the behavior of DK7. The fact that the slight f_{O_2} dependence is uniform over a range of 5 log f_{O_2} units again suggests that a single f_{O_2}-dependent mechanism controls the f_{O_2} dependence over this entire range. As in the case of DK7 diopside, two or more mechanisms could operate if their proportionate contribution remained constant, but this would again be a highly coincidental situation. The enhanced conductivity of MAL diopside is probably associated with the substitution of Fe for Mg. One possible reaction that does

not depend upon f_{O_2} (and is not likely to have a limited range with respect to f_{O_2}) is the thermal ionization of Fe^{2+} to form Fe^{3+} plus electrons in the conduction band:

$$Fe_{Mg}^{\times} = Fe_{Mg}^{\cdot} + e'$$

The activation energy (1.04 eV, Table 5) derived from our measurements of MAL diopside is relatively small and consistent with this suggestion.

The fact that MAL diopside is more conducting than DK7 does not signify that a reaction to form oxygen vacancies does not operate in MAL diopside, but it does indicate that the electrons associated with oxygen vacancies are no longer the dominant defects for electrical conduction. It is likely that the concentration of oxygen vacancies in MAL still varies with f_{O_2} but is obscured by much greater concentrations of another defect. Indeed, the smallest f_{O_2} dependence anticipated by Stocker (1978a) is $\partial(\log \sigma)/\partial(\log f_{O_2}) = -0.071$, a much larger dependence than the value we observed for MAL diopside. Thus we suggest that the conductivity of MAL diopside can be explained by a combination of two mechanisms. The effect can be shown in a simplified diagram of defect-concentration isotherms in $\log c_i - \log f_{O_2}$ space (Fig. 9). The contribution due to conduction by the f_{O_2}-independent defect is much greater than the contribution due to oxygen vacancies. The total charge-carrier concentration, the sum of the two contributions, has a slightly negative slope, similar to that observed. By measuring additional diopsides with different Fe/(Mg + Fe) values but otherwise similar chemistries, it should be possible to confirm the suggestion that ionization of Fe^{2+} is the source of the enhanced conductivity.

Ideally, activation energy refers to a process that is thermally activated. We calculated f_{O_2}-independent activation energies that range from 2.01 to 2.20 eV (and average 2.12 eV) in the DK diopside. (We calculated the energy at constant f_{O_2} rather than along an f_{O_2}-T path defined by an oxygen buffer, as might be done if there were evidence that the defect-forming reaction were dependent upon an Fe^{2+}-Fe^{3+} equilibrium with a positive value of $\partial(\log \sigma)/\partial(\log f_{O_2})$, or along a path defined by a constant gas-mixing ratio.) However, we suspect that this energy does not solely reflect a thermally activated process. The temperature dependence of the equilibrium constant K in the oxygen-defect–forming reaction will cause the bulk composition (stoichiometry) of the diopside to slightly vary with temperature, yet we know neither the diopside composition nor the activities of the species in the equilibrium. Thus the activation energy calculated from our measurements may have two components: a major component due to pure thermal activation and a minor apparent component due to the slight change in bulk composition as oxygen passes between the sample and furnace atmosphere. Comparison of our result with other reported activation energies may be ambiguous, especially if the thermally activated processes are dependent on f_{O_2}. To illustrate this ambiguity, we report an f_{O_2}-independent activation energy of 2.1 eV for DK7 at $T > 1000$ °C and compare this result with calculated activation energies of 1.4 eV along the fayalite-magnetite-quartz buffer and of 1.3 eV at a CO/CO_2 gas mixed in the proportions 10/90. Detailed measurements revealed a transition at 1000 °C and a smaller activation energy (1.3 eV, Fig. 7) at lower temperatures. Because DK7 diopside is such a poor conductor at these lower temperatures, we were not able to invetigate whether or not this activation energy is also associated with the strong f_{O_2} dependence of conductivity that is observed at higher temperatures.

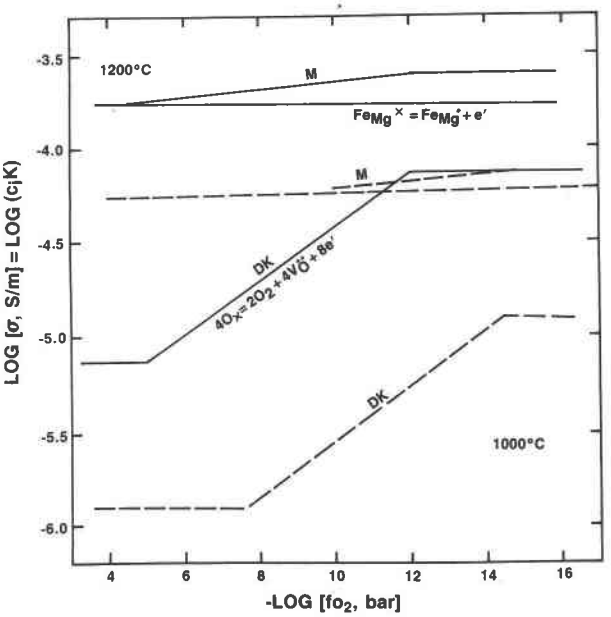

Fig. 9. Simplified diagram showing selected relationships between conductivity and f_{O_2} of diopside. Conductivity is the product of concentration and a constant (K) that incorporates mobility (see text). Light solid (1200 °C) and dashed (1000 °C) lines represent components of conductivity (lower two lines) and the sums (uppermost line) of the components. The observed conductivity of MAL diopside with Fe/(Mg + Fe) = 0.127 can be broken into two components: the f_{O_2}-dependent conductivity observed for diopside DK7 [Fe/(Mg + Fe) = 0.027] and an f_{O_2}-independent component. Point-defect reactions that might determine each component of conductivity are suggested.

The activation energy for MAL diopside at $T > 1050$ °C is 1.0 eV, distinctly less than that of the more magnesian DK7 diopside. In veiw of the different conduction mechanisms, we had anticipated a different activation energy. The increase in activation energy to 2.4 eV in the temperature range 1050 to 800 °C (and perhaps even lower temperatures) is disturbing because this increase cannot be simply explained by two mechanisms, one of which is dominant at high temperature, the other dominant at low temperature. The obvious explanation is a structural transition, but we are not aware that diopside-hedenbergite has any transition in this temperature range. The nature of the transition in MAL diopside remains unknown.

The diopside plates responded systematically and rapidly to changes in the furnace f_{O_2}. If the transport of oxygen through the diopside is by chemical diffusion across the surfaces of the plates, and if the change in conductivity is linearly proportional to the change in oxygen content of the diopside, the change in conductivity with time (Fig. 4) is a measure of the transport progress variable. It is possible to calculate a rate constant for this process, using Figure 4.6 of Crank (1975), and if that rate is controlled by bulk diffusion (rather than some process at the interface), the rate constant is a diffusion coefficient. This method does not require knowledge of the absolute concentration of the diffusing species. The rates calculated from curves 5 and 7 of Figure 4b are surprisingly fast: 9×10^{-8} cm^2/s at 1000 °C and 3×10^{-7} cm^2/s at 1200 °C. The curves are not linear when plotted as σ and $t^{-1/2}$, suggesting that the rates are not controlled solely by diffusion. Thus the actual diffusion rates would be somewhat faster than the rates calculated from the equation of Crank (1975). These rates seem unreasonably fast. For comparison, the oxygen self-diffusion rate in synthetic forsterite, Fo_{100}, ranges from 10^{-16} cm^2/s at 1200 °C to 10^{-18} cm^2/s (extrapolated) at 1000 °C (Jaoul et al., 1983). For natural olivine, Fo_{89}, oxygen self-diffusion is faster than in Fo_{100} by a factor of 100 to 1000 (Houlier et al., 1985). The direct measurements of the oxygen self-diffusion rates in olivine are so much slower than our indirectly determined rates in diopside that we conclude that our rates are not oxygen-diffusion coefficients.

If the oxygen vacancies are assumed to be the charge-carrying species, it is possible to calculate a diffusion coefficient from the conductivity

$$D_i = \sigma RT/c_i z^2 F^2$$

(Tuller, 1985, Eq. 4) using representative values of conductivity [10^{-5} S/m or s^3·A^2/(m^3·kg)], temperature (1373 K), concentration (5.4×10^3 mol/m^3), and valence (2) and expressing the gas and Faraday constants in base units [8.314 m^2·kg/(s^2·K·mol) and 96485 A·s/mol, respectively]. The resulting value of D is 2.3×10^{-11} cm^2/s, larger than the oxygen diffusion rate in olivine and, surprisingly, larger than the Ca-(Mg,Fe) diffusion rate in pyroxenes (Huebner and Voigt, 1984). If our oxygen-vacancy concentration is overestimated, the calculated diffusion coefficient would be even larger. Thus, the relatively large calculated diffusion coefficient leads us to suspect that the initial assumption is incorrect and to suggest that electrons, not oxygen vacancies, are the charge-carrying species.

These results have important implications for understanding crystal chemistry and chemical diffusion in pyroxenes. One might have anticipated that the SiO_4 unit in pyroxene would be so tightly bonded that oxygen vacancies would be energetically unfavorable defects and that changes in the oxygen content would be exceedingly slow because of slow diffusion rates. Further, although there is convincing evidence for cation vacancies in clinopyroxenes at high pressures (Wood and Henderson, 1978; Smyth, 1980; Gasparik, 1984), we commonly assume that at low pressure, pyroxenes have cation : anion ratios exactly equal to 4:6. Our results suggest that this assumption is incorrect. If the observed change in density with f_{O_2} is due solely to change in oxygen content, which appears to be likely, the measured density changes of 0.5% and 0.9% correspond to gain or loss of 1.1% and 2.0% of the oxygen atoms present, or 0.13 and 0.24 charges, respectively, per six-oxygen formula unit. Changes of this magnitude will invalidate Fe^{2+}/Fe^{3+} ratios calculated assuming perfect four-cation to six-oxygen stoichiometry. For instance, a change of ± 0.20 charges will affect the calculated valence of 50% of the Fe atoms of a pyroxene of nominal composition $Ca_{0.8}Mg_{0.8}Fe_{0.4}Si_2O_6$!

The DK7 diopside equilibrated rapidly and reversibly with respect to changes in the f_{O_2} of the furnace atmosphere. Because Reactions 3 and 4 each require the passage of oxygen or oxygen vacancies through pyroxene, it appears that migration of oxygen or oxygen vacancies in DK7 diopside is a relatively rapid process, observable on a time scale of hours. If the migration path is by bulk diffusion, it contrasts with the much slower bulk diffusion of Ca, Mg, Fe, Sr, and Sm cations in diopside (Huebner and Voigt, 1984; Sneeringer et al., 1984) and calls into question the common assumption that the oxygen ions or SiO_4 groups form a rigid and immobile framework. Conversely, some oxygen migration might occur along dislocations. Nevertheless, our proposed oxygen vacancies provide a possible chemical diffusion mechanism for pyroxenes. The large Ca cation is a principal diffusing species during exsolution in pyroxenes, yet without large vacancies, it is difficult to imagine Ca diffusion through the pyroxene lattice. The proposed oxygen vacancies would form a possible migration path for Ca, Mg, and Fe cations. Finally, our results provide some insight for choosing values of experimental parameters when attempting to measure diffusion rates. Surprisingly, use of relatively low f_{O_2} values may enhance cation diffusion in Fe-bearing pyroxenes. We did not observe the positive dependence of electrical conductivity on oxygen fugacity that would occur if $Fe^{\times}_{Mg}$ was oxidized to $Fe^{\cdot}_{Mg}$ through a process that changed the bulk composition, and we would not expect this reaction to cause the large vacancies that Mg, Fe, and particularly Ca ions must require for diffusion. Instead, diffusion may best be promoted by the relatively reducing conditions that produce oxygen vacancies. To hasten slow-diffusion reactions, experimental studies of diffusion should be attempted at low f_{O_2} values, even in Fe-bearing systems.

Our results are surprisingly complicated but are incomplete and indicate directions for future research. The behavior of MAL diopside, with a small activation energy at high temperature and a larger activation energy at low temperature, indicates the presence of a reversible transition that will introduce a new mechanism at 1050 °C. High-temperature (900–1200 °C) unit-cell and calorimetric measurements might reveal the presence of a transition in MAL and other diopsides. Extrapolation of trends

observed at high temperature is necessary if our results are to be used as models of behavior in the metamorphic temperature range, yet we have no confidence that these extrapolations are justified. In particular, we cannot be confident that the f_{O_2} dependence of conductivity, and thus the oxygen-vacancy model of diffusion, is appropriate at $T < 1000$ °C. One wonders whether or not other silicates will have as many conductivity regimes as does diopside. We know very little about the absolute concentrations of any point defects in silicates and how these concentrations change in response to f_{O_2}. Were their concentrations to be determined, thermogravimetrically and as a function of time, one could extract diffusion rates (from the rate of change in mass) and mobilities of charge carriers from the data.

Our results will provide a basis for validating the use of aggregates to determine bulk or single-crystal properties. Unlike the limited selection of composition provided by natural samples, synthetic aggregates make it possible to vary a single cation ratio (useful in identifying defect mechanisms), to define the activity or activity ratio of components by means of additional phases that are dispersed to promote rapid achievement of equilibrium, and to study the grain-boundary component of conduction. The biggest uncertainty in the use of pyroxene aggregates has concerned possible conduction along grain boundaries. By comparing measurements made on aggregates of DK diopside under different conditions with the "isotropic" conductivity obtained by averaging the conductivity in three orientations of DK7 (Table 5), it should be possible to distinguish the components of bulk and grain-boundary conduction and to test the hypothesis that "isotropic" bulk conductivity measurements can be obtained from aggregates.

Acknowledgments

Through generous cooperation, numerous people made contributions to this study. Vandall King of Ward's Geoscience Establishment arranged for the collection of the diopside crystals from De Kalb, New York. Daniel Appleman of the Mineral Sciences Department, U.S. National Museum of Natural History, agreed in principle to acquire large quantities of crystals that could be shared by the mineralogical and geophysical research community and, in the case of the De Kalb crystals, did so. Al Duba of the Lawrence Livermore Laboratory kindled the first author's interest in electrical conductivity. Rosemary Knight of Stanford University first drew his attention to impedance spectroscopy techniques, and Ian Raistrick, also of Stanford, provided early advice about the necessary equipment. Brian Seegmiler of the Coors Porcelain Company made it possible for us to acquire the insulating Vistal rods used to support the sample cell in the furnace. F. L. Harmon of the USGS manufactured the complicated furnace fittings. Randall Cygan of the University of Illinois acted as a sounding board for our interpretations of the spectral signatures; Cygan, Gordon L. Nord, Jr., of the U.S. Geological Survey, Robrt N. Schock and Al Duba of the Lawrence Livermore Laboratory, and an anonymous reviewer for the journal all reviewed the manuscript and provided helpful suggestions.

References cited

Bence, A.E., and Albee, A.L. (1968) Empirical correction factors for the electron microanalysis of silicates and oxides. Journal of Geology, 76 382–403.

Busing, W.R., and Levy, H.A. (1962) ORGLS: A general least squares program. U.S. Atomic Energy Commission, Oak Ridge National Laboratory, ORNL-TM-271, 39 pages. [An updated version is reproduced in Baes, C.F., Jr., and Mesmer, R.E. (1976) The hydrolysis of cations, p. 443–458. Wiley, New York.]

Cemic, L., Will, G., and Hinze, E. (1980) Electrical conductivity measurements on olivines Mg_2SiO_4-Fe_2SiO_4 under defined thermodynamic conditions. Physics and Chemistry of Minerals, 6, 95–107.

Crank, J. (1975) The mathematics of diffusion. Clarendon Press, Oxford.

Deines, Peter, Nafziger, R.H., Ulmer, G.C., and Woerman, Eugene. (1974) Temperature-oxygen fugacity tables for selected gas mixtures in the system C-H-O at one atmosphere total pressure. Pennsylvania State University Bulletin of the Earth and Mineral Sciences Experiment Station, 88, 129 p.

Duba, A., and Nicholls, I.A. (1973) The influence of oxidation state on the electrical conductivity of olivine. Earth and Planetary Science Letters, 18, 59–64.

Duba, A., Boland, J.N., and Ringwood, A.E. (1973) The electrical conductivity of pyroxene. Journal of Geology, 81, 727–734.

Duba, A., Heard, H.C., and Schock, R.N. (1974) Electrical conductivity of olivine at high pressure under controlled oxygen fugacity. Journal of Geophysical Research, 79, 1667–1673.

——— (1976) Electrical conductivity of orthopyroxene to 1400°C and the resulting selenotherm. Proceedings of the 7th Lunar Science Conference, 3173–3181.

Duba, A., Dennison, M., Irving, A.J., Thornber, C.R., and Huebner, J.S. (1979) Electrical conductivity of aluminous orthopyroxene. Lunar and Planetary Science X, p. 318–319. Lunar and Planetary Institute, Houston, Texas.

Dvorak, Z., and Schloessin, H.H. (1973) On the anisotropic electrical conductivity of enstatite as a function of pressure and temperature. Geophysics, 38, 25–36.

Gasparik, Tibor. (1984) Experimental study of subsolidus phase relations and mixing properties of pyroxene in the system CaO-Al_2O_3-SiO_2. Geochimica et Cosmochimica Acta, 48, 2537–2545.

Hinze, E., Will, W., and Cemic, L. (1981) Electrical conductivity measurements on synthetic olivines and on olivine, enstatite and diopside from Dreiser Weiher, Eifel (Germany) under defined thermodynamic activities as a function of temperature and pressure. Physics of the Earth and Planetary Interiors, 25, 245–254.

Houlier, B., Jaoul, O., and Lieberman, R.C. (1985) Oxygen and silicon self-diffusion in natural olivine: First data at $T = 1300$ °C. EOS, 66, 372.

Huebner, J.S. (1975) Oxygen fugacity values of furnace gas mixtures. American Mineralogist, 60, 815–823.

——— (1987) Use of gas mixtures at low pressure to specify oxygen and other fugacities of furnace atmospheres. In Ulmer, G.C. and Barnes, H.L., Eds., Hydrothermal experimental techniques, p. 20–60. Wiley, New York.

Huebner, J.S., and Papike, J.J. (1970) Synthesis and crystal chemistry of sodium-potassium richterite, $(Na,K)NaCaMg_5Si_8O_{22}(OH,F)_2$: A model for amphiboles. American Mineralogist, 55, 1973–1992.

Huebner, J.S., and Voigt, D.E. (1984) Chemical diffusion in Ca-Mg-Fe pyroxenes: Measured rates of cation exchange and interface movement. Geological Society of America Abstracts with Programs, 16, 546.

Huebner, J. S., and Woodruff, M.E. (1985) Chemical compositions and critical evaluation of microprobe standards available in the Reston microprobe facility. U.S. Geological Survey Open File Report 85-718.

Huebner, J.S., Duba, A., and Wiggins, L.B. (1979) Electrical conductivity of pyroxene which contains trivalent ions: Laboratory measurements and the lunar temperature profile. Journal of Geophysical Research, 84, 4652–4656.

Jaoul, Olivier, Houlier, Bernard, and Abel, Francois. (1983) Study of ^{18}O diffusion in magnesium orthosilicate by nuclear microanalysis. Journal of Geophysical Research, 88, 613–624.

Kushiro, Ikuo. (1972) Determination of liquidus relations in synthetic silicate systems with electron probe analysis: The system forsterite-diopside-silica at 1 atmosphere. American Mineralogist, 57, 1260–1271.

Kröger, F.A. (1974) Chemistry of imperfect crystals, vol. 2. North Holland, Amsterdam.

Maury, R. (1968) Conductibilité électrique des tectosilicates I. Méthode et résultats expérimentaux. Bulletin de la Société Française Minéralogie et Cristallographie, 91 267–278.

Parkhomenko, E.I. (1982) Electrical resistivity of minerals and rocks at high temperature and pressure. Reviews of Geophysics and Space Physics, 20, 193–218.

Pluschkell, W., and Engell, H.J. (1968) Ionen- Und Elektronenleitung im Magnesiumorthosilikat. Berichte der Deutschen Keramischen Gesellschaft, 45, 388–394.

Rickert Hans. (1982) Electrochemistry of solids. Springer-Verlag, New York.

Schock, R.N., Ed. (1985) Point defects in minerals. American Geophysical Union Geophysical Monograph 31.

Schock, R.N., and Duba, A.G. (1985) Point defects and the mechanisms of conduction in olivine. American Geophysical Union Geophysical Monograph 31, 88–96.

Smyth, J.R. (1980) Cation vacancies and crystal chemistry of breakdown reactions in kimberlitic omphacites. American Mineralogist, 65, 1185–1191.

Smyth, D.M., and Stocker, R.L. (1978) Point defects and non-stoichiometry in forsterite. Physics of the Earth and Planetary Interiors, 10, 183–192.

Sneeringer, Mark, Hart, S.R., and Shimizu, Nobumichi. (1984) Strontium and samarium diffusion in diopside. Geochimica et Cosmochimica Acta, 48, 1589–1608.

Stocker, R.L. (1978a) Variation of conductivity in enstatite with oxygen partial pressure: Comparison of observed and predicted behavior. Physics of the Earth and Planetary Interiors, 17, P34–P40.

——— (1978b) Point defect formation parameters in olivine. Physics of the Earth and Planetary Interiors, 17, 108–117.

Stocker, R.L., and Smyth, D.M. (1978) Effect of enstatite activity and oxygen partial pressure on the point-defect chemistry of olivine. Physics of the Earth and Planetary Interiors, 16, 145–156.

Tuller, H.L. (1985) Electrical conducion in ceramics: Toward improved defect interpretation. American Geophysical Union Geophysical Monograph 31, p. 47–68.

Voigt, R., Seifert, K.F., and Will, G. (1979) Die elektrische Leitfahigkeit von Pyroxenen der Reihe $MgSiO_3$-$FeSiO_3$ bei 10 und 20 kbar unter definierten thermodynamischen Bedingungen. Neues Jahrbuch für Mineralogie Monatshefte, 296–308.

Will, G., Cemic, L., Hinze, E., Seifert, K.-F., and Voigt, R. (1979) Electrical conductivity measurements on olivines and pyroxenes under defined thermodynamic activities as a function of temperature and pressure. Physics and Chemistry of Minerals, 4, 189–197.

Wood B.J., and Henderson, C.M.B. (1978) Compositions and unit cell parameters of synthetic non-stoichiometric tschermakitic clinopyroxene. American Mineralogist, 63, 66–72.

Manuscript received November 20, 1987
Manuscript accepted July 12, 1988